UNIVERSITY OF OKLAHOMA

GRADUATE COLLEGE

EXAMINATION OF ADDITIVELY MANUFACTURED CHOKES FOR SIZE REDUCTION AND PERFORMANCE IMPROVEMENT IN RF AND MICROWAVE APPLICATIONS

A THESIS

SUBMITTED TO THE GRADUATE FACULTY

in partial fulfillment of the requirements for the

Degree of

MASTER OF SCIENCE

By

DAVID MITCHELL
Norman, Oklahoma
2018

EXAMINATION OF ADDITIVELY MANUFACTURED CHOKES FOR SIZE REDUCTION AND PERFORMANCE IMPROVEMENT IN RF AND MICROWAVE APPLICATIONS

A THESIS APPROVED FOR THE
SCHOOL OF ELECTRICAL AND COMPUTER ENGINEERING

BY

Dr. Jessica Ruyle, Chair

Dr. Caleb Fulton

Dr. Hjalti Sigmarsson

Acknowledgements

I would like to thank Dr. Jessica Ruyle, without her guidance this work would not have been possible. Additionally, I would like to thank Dr. Caleb Fulton and Dr. Hjalti Sigmarsson.

Contents

List of Figures

List of Tables

Abstract

For many RF and microwave applications, a balun is imperative to ensure the proper performance of a balanced structure that is connected to an unbalanced structure. Sleeve baluns are a common type of balun that are relatively cheap and basic, but they are also large, heavy, and time consuming to assemble. This works presents several novel methods of using additive manufacturing techniques to mitigate all of these issues. First, a methods of 3D printing basic designs to reduce weight and improve ease of assembly is presented. This method is then used to construct balun with up to two folds, which reduces the overall size of the balun with each consecutive fold. Next, a castable silicone is used to also reduce the overall size of a balun by reducing the effective wavelength on the balun's interior, which is first tested with traditional unfolded baluns. This method was then combined with the folded balun design to compound the size reduction from both methods. A final method of printing a dielectric core and applying metal to the core is then presented. The performance of all of the baluns is presented and discussed and future improvements are addressed. Ultimately, this work establishes a method of drastically reducing the size of sleeve baluns to a point where they can be used as in line components, while still maintaining performance levels comparable to a standard, bulky sleeve balun.

Chapter 1

Introduction

In almost all complex RF and microwave systems, a balanced structure must inevitably be connected to an unbalanced structure due to the ubiquitous use of coaxial cable [1, 2]. Almost any signal generator, network analyzer, or amplifier will use coax to carry the signal. This cable provides an excellent low-loss means of carrying TEM signals [3], but coax is inherently an unbalanced structure [4]. Currents travelling on the outer conductor can flow on either the interior or exterior surface, creating unbalanced current distributions. These imbalances can lead to impedance mismatches, power reflection, and radiating cable currents when a balanced structure is directly connected, leading to deteriorated performance by the balanced structure [4–8]. A component designed to ensure the designed performance at these connection points is known as a balun, because it connects a BAL-anced structure to an UN-balanced structure [4, 5, 9]. At low frequencies, cutoff around 100 MHz, ferrite beads accomplish this by presenting a large, lossy impedance to the currents on the exterior of the coax [1, 8, 10]. Above these frequencies, though, ferrite beads do not work effectively and other balun types are necessary [2, 7]. One such balun is a sleeve balun. Sleeve baluns are a commonly used type of balun at these frequencies because their construction is

relatively cheap and simple. They can be made using just a piece of copper pipe and a sheet of copper. These baluns do have several disadvantages, however. As was established in [4–7, 9], they must be roughly a quarter wavelength long, making them relatively bulky. Their assembly also requires the use of extremely high heat as the copper pipe acts a large heat sink, preventing the use of normal soldering techniques. These baluns must also be assembled by hand one at a time, which can take significant amount of time and can easily lead to inconsistencies in quality. Special milling equipment would also be needed to construct a balun like this, which eliminates the capability of using computer aided machinery in most applications.

There have been some attempts to improve the shortcomings of sleeve baluns. Sleeve baluns have been folded a single time in order to reduce the overall length by roughly half [5, 6], but this does not alleviate the issues of weight or fabrication intensity. They also have not been folded more than a single time due to prohibitively difficult construction. Conversely, all of these issues can be significantly reduced with additive manufacturing techniques, which is, generally, the process of constructing a component by adding material, as opposed to subtractive manufacturing where a component is constructed by removing material, such as in milling. For example, the materials used in these techniques are inherently lighter than the copper pipe used for traditional sleeve baluns. Furthermore, structures that would be prohibitively difficult, if not outright impossible, to build using traditional materials are straightforward to build using additive manufacturing techniques, provided proper design considerations are made. The double folded balun seen in Fig. 1.1, whose design and construction is detailed in Section 5.2.2, is an example of such a structure. These baluns can also be made in large batches without increasing the necessary time by a significant amount. This work

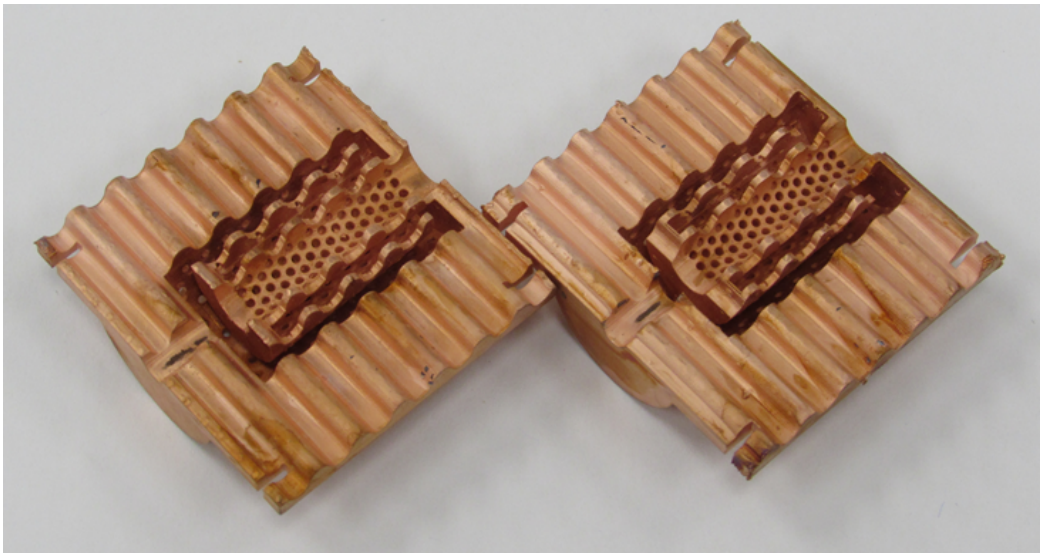

FIGURE 1.1: An example of the two halves of a double folded balun that was printed and plated with copper, with a standard American 25¢ coin for reference. Its construction will be detailed in Section 5.2.2.

investigates several such methods of using additive manufacturing techniques to greatly diminish all these detriments of traditional sleeve baluns and achieve a final component that is a fraction of the weight and size of a traditional balun.

This thesis will first begin with an overview of the functionality and important aspects of sleeve baluns is given in Chapter 2. Next, an overview of additive manufacturing and its applications in RF and microwave applications is given in Chapter 3. A comparison of the performance of additively manufactured sleeve baluns to the performance of traditionally manufactured sleeve baluns is also presented in Chapter 4. Next, in Chapter 5, the principles of a folded balun are detailed. Printed baluns with a single fold are then described to support this. These ideas are then extended to baluns with two folds in Section 5.2.2. Chapter 6 then introduces another method of size reduction, substrate integration. This method is first tested using two types of pourable silicone with unfolded copper pipe baluns and then, once the concept is verified, with double folded baluns to compound the size reduction effects of the folding and the dielectric. Section

6.2 presents another method of producing substrate integrated baluns using 3D printed cores that allows for the widely accessible production of baluns. Finally, Chapter 7 draws overall conclusions for the work and gives areas for potential future work.

Chapter 2

Sleeve Baluns

2.1 Introduction

This chapter will detail the basic functionality of sleeve baluns and how additive manufacturing techniques can be applied to their construction. First, a figure of merit for the performance of baluns, Common Mode Rejection Ratio, is given. This chapter then goes on to give a breakdown of the different aspects of a sleeve balun and how each aspect affects the performance and operating frequency of the balun, which will come into play with later designs. Next, a 3D printed sleeve balun is compared to a traditionally manufactured copper pipe sleeve balun to test the viability of additive manufacturing in this application. Their performances are discussed and conclusions are then given.

2.2 Background

Baluns in general are a type of component used for connecting balanced structures, such as a dipole antenna, to unbalanced structures, such as coaxial cable in order to prevent impedance mismatches and radiation on the feed cable. Sleeve baluns are a commonly used type of balun because their construction is relatively cheap and simple, being commonly composed of just a piece of copper pipe and a sheet of copper. In the example of a dipole antenna connecting to coax, illustrated in Fig. 2.1, a sleeve balun could be used to ensure proper current distributions and proper radiation [4, 6]. The sleeve balun presents a large impedance to the currents flowing on the exterior of the outer conductor of the coax, known as the common mode currents and labeled I_C in Fig. 2.1, and significantly reduces them [6]. Common Mode Rejection Ratio (CMRR) is a measure of this reduction and is a standard figure of merit for the performance of baluns [6, 11]. CMRR can be measured using a differential probe, seen in the expanded portion of Fig. 2.2. This jig allows for the direct measurement of CMRR using a multi-port network analyzer by converting the normally two port network into a three port network [6, 11]. With this probe attached as in Fig. 2.2, Port 2 is associated with currents on the outer conductor of the coax (I_B and I_C in Fig. 2.1) and Port 3 is associated with currents on the inner conductor (I_A in Fig. 2.1). From the three-port measurement, with the ports assigned as labeled in Fig. 2.2, the CMRR can be found by

$$CMRR(dB) = 20 \times \log\left(\frac{S_{21} + S_{31}}{S_{21} - S_{31}}\right), \tag{2.1}$$

where S_{21} and S_{31} are three port scattering parameters of the setup shown in Fig. 2.2 [11]. If $I_C = 0$ and $I_B = I_A$, it then follows that $S_{21} = S_{31}$. The CMRR

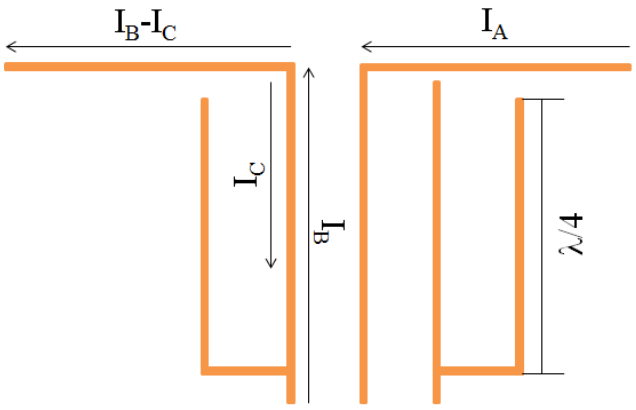

FIGURE 2.1: An illustration of the current distributions in a system consisting of a dipole connected to a length of coax with a sleeve balun attached, where I_A is the current flowing on the center conductor of the coax, I_B is the current flowing on the interior of the outer conductor, and I_C is the current flowing on the exterior of the outer conductor. I_C is also more specifically called the common mode current.

as given by Equation 2.1 would then be infinite. Therefore, CMRR can be used to determine the performance of a balun, with a large value indicating that the common mode currents are being effectively choked. Small variations in S_{21} and S_{31} from any source, such as the quality of the solder connecting the wires or the noise floor of the network analyzer, will significantly degrade the level of this measurement, however. Therefore, a CMRR of greater than 38 dB will be considered adequate for this work because it shows a less than 3% difference between S_{21} and $S)31$.

Insertion loss may also be found using this measurement setup. The total power, P_{total}, input into the system will be equal the reflected power added to the transmitted power, or

$$P_{total} = |S_{11}|^2 + |S_{21}|^2 + |S_{31}|^2, \tag{2.2}$$

where S_{11}, S_{21}, and S_{31} are the three port scattering parameters of the measurement setup in Fig. 2.2. The square root of this value can then be treated as

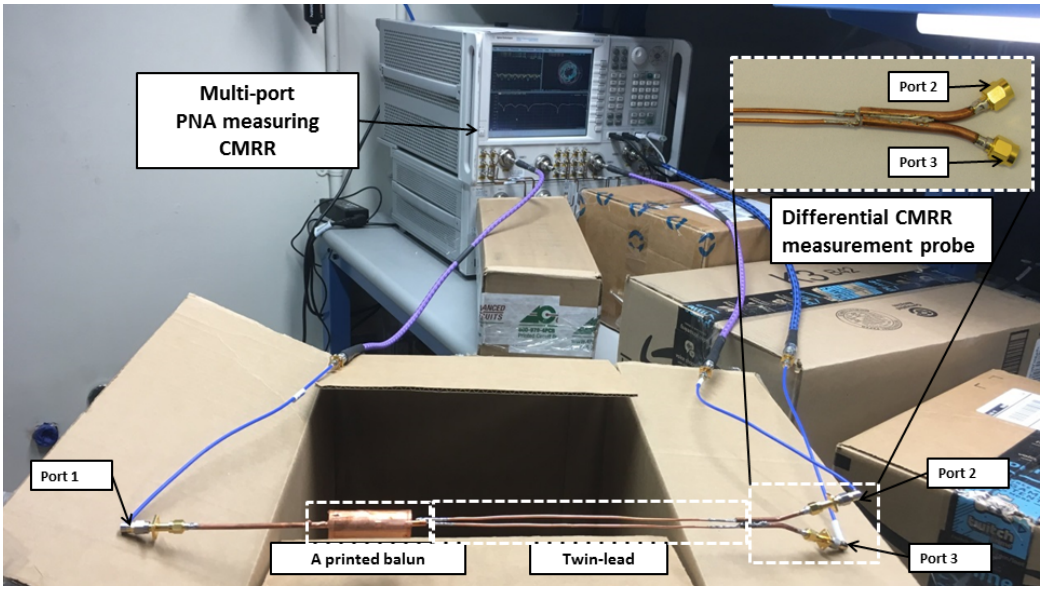

FIGURE 2.2: The full measurement setup using a multi-port PNA with a printed balun connected to a differential probe via a length of twin lead.

the Insertion Loss, or the of power that occurs while travelling through a device. This not the true Insertion Loss of the balun because it would be prohibitively difficult to de-embed the measurements to the plane of the balun. It is still a useful measurement, however, because it can be compared against a measurement from the same setup without a balun attached, seen in Fig. 2.3, in order to evaluate the performance of a balun at its operating frequency.

While they are simple and useful structures, sleeve baluns do have several disadvantages. As will be discussed in Section 2.3, they must be a quarter wavelength long, making them relatively bulky. Their assembly also requires the use of extremely high heat as the copper pipe acts a large heat sink, preventing the use of normal soldering techniques. Finally, they must also be manually tuned to achieve the exact desired operational frequency.

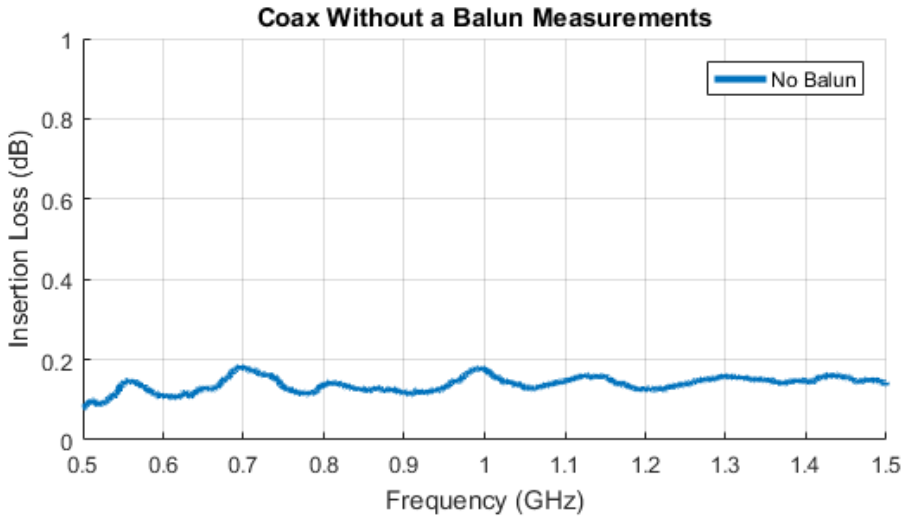

FIGURE 2.3: The Insertion Loss of a length of coax connected to the differential probe with no balun connected.

2.3 Functionality

A sleeve balun can be broken down into four main aspects that determine its performance: its overall length, the properties of the short, the bulk properties of the conductors, and the spacing between the opening of the balun and the point of connection between the balanced and unbalanced structures. The contributions and importance of each of these aspects will be shown.

2.3.1 Length

The first property, the overall length, l, plays the largest role in determining the operational frequency of the balun. The outer conductor of the semi-rigid coax and the copper pipe of the balun form a length of coaxial cable transmission line. The input impedance, Z_{choke}, at the opening of the balun, shown in Fig. 2.4, can then be determined using the well-established relation of impedance of a lossless transmission line,

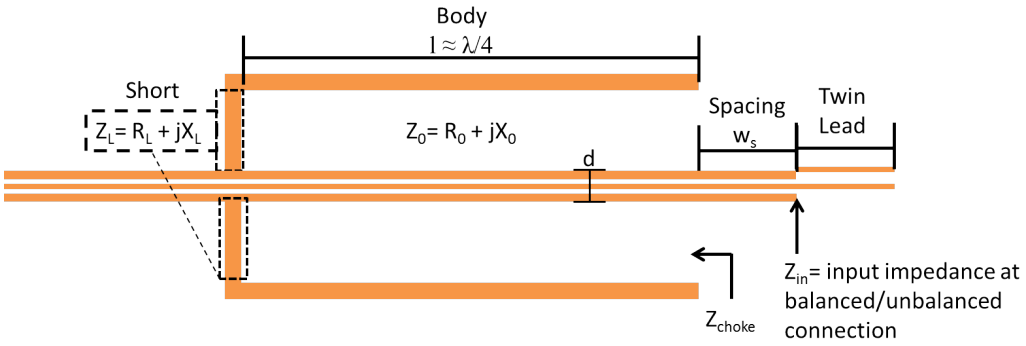

FIGURE 2.4: A diagram of a balun with lengths and impedance values labeled, where Z_{choke} is the input impedance of the balun, Z_0 is the characteristic impedance of the balun, Z_L is the impedance of the short, w_s is the spacing between the opening of the balun and the point where the coax would connect to a balanced structure, and Z_{in} is the impedance at the point of connection with a balanced structure.

$$Z_{choke} = Z_0 \frac{Z_L + jZ_0 tan(\beta l)}{Z_0 + jZ_L tan(\beta l)}, \tag{2.3}$$

where Z_0 is the characteristic impedance of the transmission line, Z_L is the impedance of the short, $\beta = 2\pi/\lambda$ is the phase constant, and l is the length. If the length is set such that $l = \frac{\lambda}{4}$, making $\beta l = \frac{2\pi}{\lambda}\frac{\lambda}{4} = \frac{\pi}{2}$, then Equation 2.3 becomes

$$Z_{choke} = Z_0 \frac{Z_L + jZ_0 tan(\frac{\pi}{2})}{Z_0 + jZ_L tan(\frac{\pi}{2})}, \tag{2.4}$$

which then approaches

$$Z_{choke} = \frac{Z_0^2}{Z_L} \tag{2.5}$$

as $\beta l \to \frac{\pi}{2}$. For this balun, Z_L is the impedance of a short, making it very small. This small impedance then makes the impedance at the opening of the balun

is extremely large and chokes the current flowing on the exterior of the outer conductor of the interior coax. This is only the case whenever the length is a quarter wavelength, however, making the length the most important aspect in determining the operational frequency.

2.3.2 Short Properties

The results of Section 2.3.1 hold true if the Z_L is assumed to be a perfect short, or purely real and very small in magnitude. This is not the case for virtually any realizable scenario. Therefore, these results must be adjusted to account for when the shorted end of the balun does not form a perfect short and has a small amount of reactance. This would be the case if holes were added to the metal, if there is a broken connection at any point, or if there is any extra material filling a corner. Assuming the short has some small resistance R_L and some small reactance X_L, making its impedance $Z_L = R_L + jX_L$, as labeled in Fig. 2.4, Equation 2.5 becomes

$$Z_{choke} = \frac{Z_0^2}{R_L + jX_L}. \tag{2.6}$$

Equation 2.6 can then be rationalized to

$$Z_{choke} = \frac{Z_0^2}{R_L^2 + X_L^2}(R_L - jX_L). \tag{2.7}$$

The effects of this reactance can be best visualized on the Smith Chart, as in Fig. 2.5. Since the short is not a perfect short, it is shifted off of the real axis along the outer circle. Therefore, a quarter wavelength away at the desired

operational frequency is not a necessary large impedance. An open is, however, some fractional wavelength more or less than a quarter of a wavelength away at a different frequency that would have the same physical length. This results in the effective operational frequency of the balun being shifted up or down depending on if the reactance of the short is capacitive or inductive, respectively.

This effect can be confirmed with simulation in ANSYS High Frequency Structure Simulator (HFSS) [12] using the length of coax seen in Fig. 2.6. A waveport was placed at the opening of the balun in order to simulate the input impedance of the length of coax. Elliptical holes were then cut in the shorted end of the coax and then the length of the major axis and the axial ratio of the ellipses as well as the number number of ellipses were varied, with examples of some of these holes seen in Fig. 2.7. The simulated input impedance was then measured and a sample of the results can be seen in Fig. 2.8. These results show that for a short with 8 holes, the peak input impedance can be adjusted within a 5 MHz range simply by varying the width of the holes.

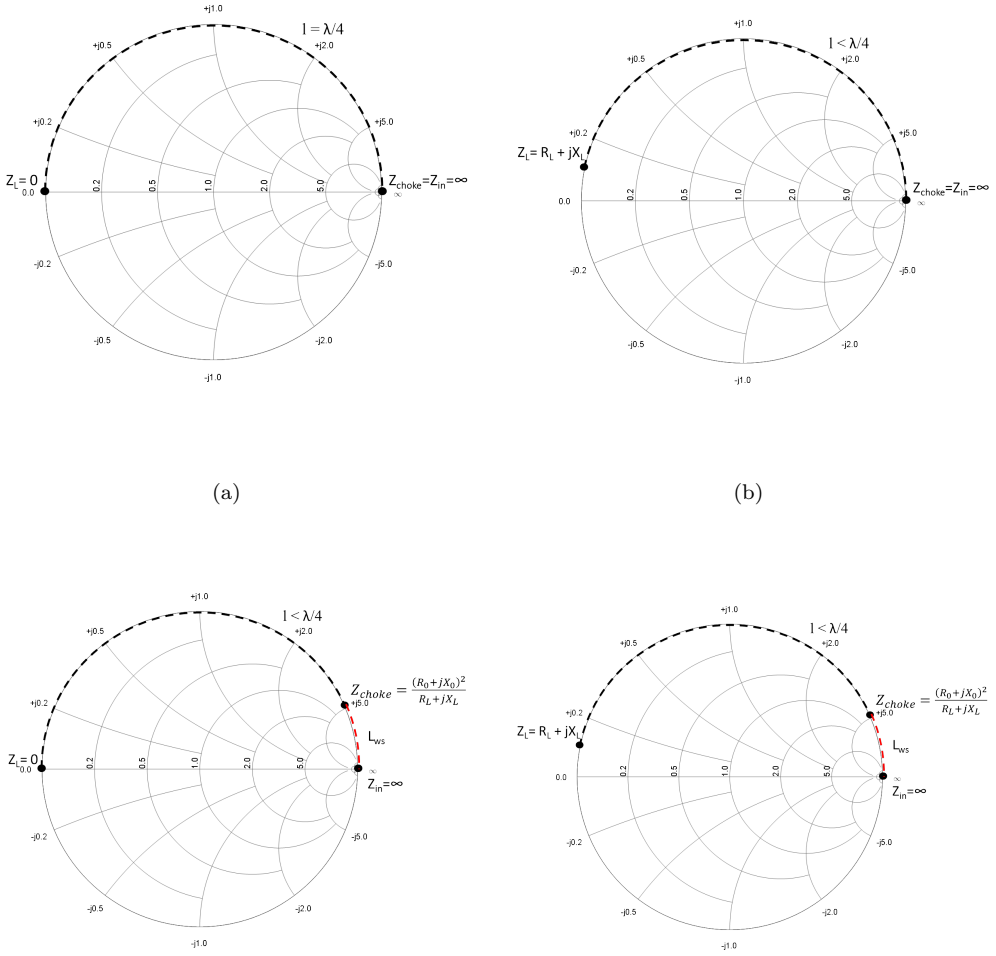

FIGURE 2.5: An illustration using a Smith Chart of the effects of a non-zero reactances. A perfect short and line with no reactance is shown in (a), a reactive short and non-reactive line is shown in (b), a perfect short with a reactive line balanced by the inductance of a wire is shown in (c), and a reactive short with a reactive line balanced by the inductance of a wire is shown in (d).

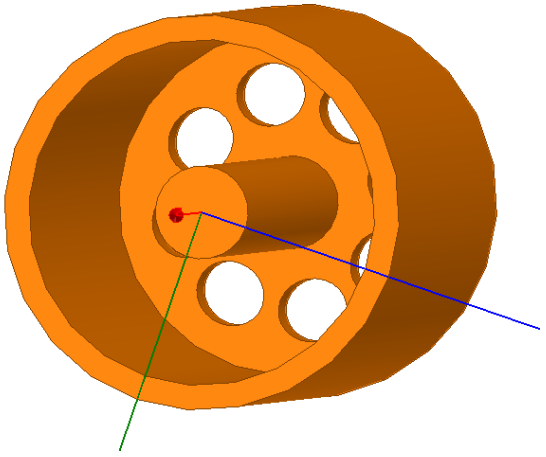

FIGURE 2.6: The simulated length of coax used to determine the effects of the size, shape, and number of holes in the shorted end of the coax.

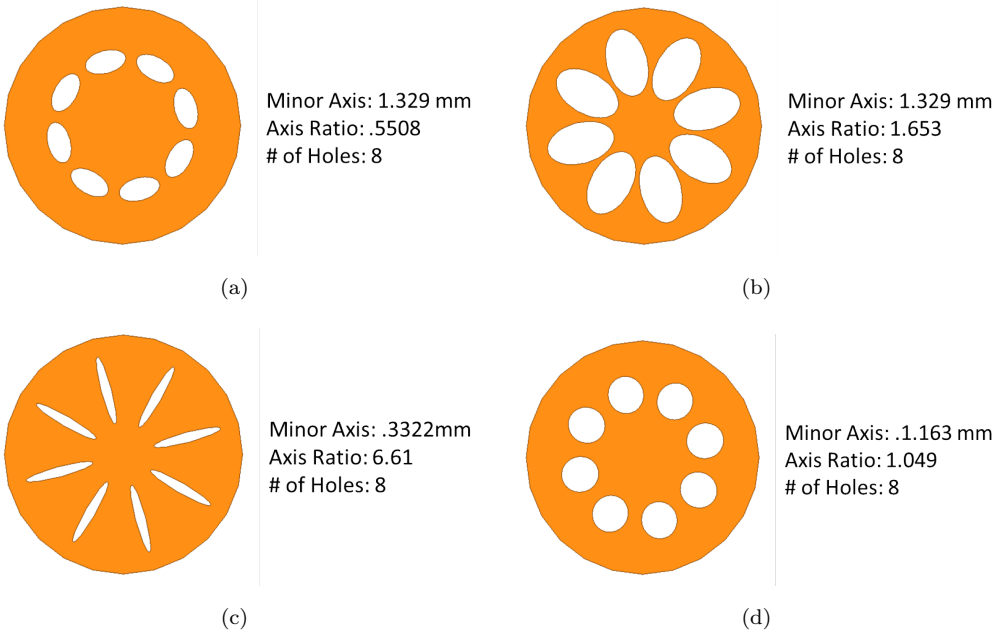

FIGURE 2.7: Some examples of the shapes of holes in the shorted end that were used, with major axis, axial ratio, and number of holes labeled.

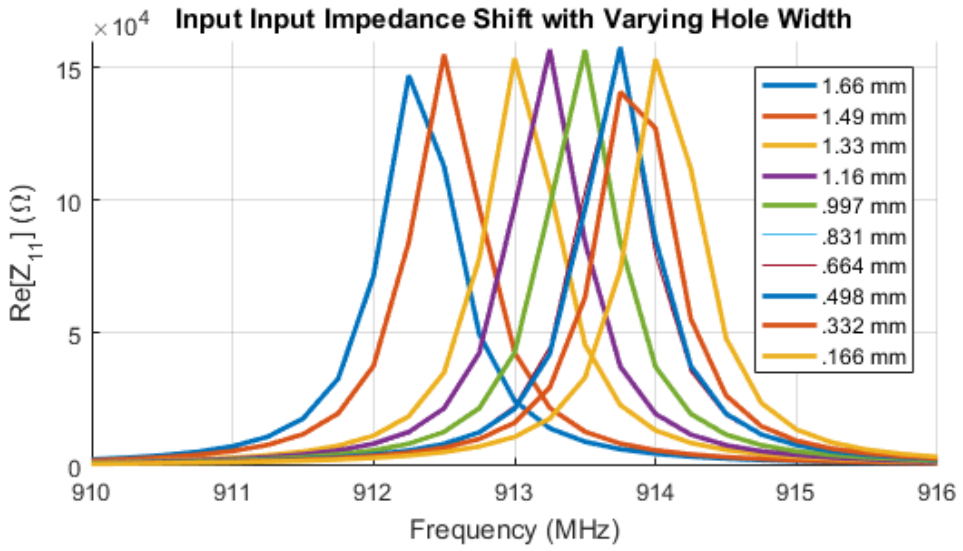

FIGURE 2.8: The input impedance of the length of shorted coax with 8 holes of minor axes varying from .166 mm to 1.661 mm with a constant major axis length.

2.3.3 Conductor Properties

Compared to the other aspects, the physical properties of the pipe that composes the balun also have a very similar effect. The characteristic impedance, Z_0, of the balun is given by

$$Z_0 = \frac{\sqrt{R + j\omega L}}{\sqrt{G + j\omega C}}, \tag{2.8}$$

where

$$R = \frac{1}{2\pi}\sqrt{\frac{\pi f \mu_c}{\sigma_c}}(\frac{1}{a} + \frac{1}{b}), \tag{2.9}$$

$$L = \frac{\mu}{2\pi}\ln\frac{b}{a}, \tag{2.10}$$

$$G = \frac{2\pi\sigma}{\ln\frac{b}{a}}, \tag{2.11}$$

and

$$C = \frac{2\pi\epsilon}{\ln \frac{b}{a}} \tag{2.12}$$

where R is the resistance of the line, L is the inductance of the line, G is the admittance of the line, C is the capacitance of the line, ω is the angular frequency, f is the frequency in Hertz, μ_c being the permeability of the conductor, σ_c being the conductivity of the conductor, μ is the permeability of the filling of the coax, ϵ is the permittivity of the filling of the coax, a is the radius of the inner conductor of the coax, and where b is the outer radius of the coax [13]. From Equations 2.8-2.12, it can be seen that the diameter of the balun greatly affects the characteristic impedance, including its reactive component. This change in the reactance would mirror the reactance changes described in Section 2.3.2, causing similar shifts in the operating frequency. This conclusion is supported by the full-wave analysis of a sleeve balun done in [9].

A similar level of influence can be seen from any holes through the body, labeled in Fig. 2.4, of the balun. Holes such as this, as seen in Section 4, would be added to improve the quality of an electroplated part. These holes can be treated as circular waveguides and, as such, would have a cutoff frequency of

$$f_{c_{11}} = \frac{1.841}{2\pi r\sqrt{\mu\epsilon}} \tag{2.13}$$

for a TE_{11} mode, which has the lowest cutoff frequency for any mode in a circular waveguide, where r is the radius of the hole, μ is the permeability in the waveguide, and ϵ is the permittivity inside the waveguide [14]. A desired cutoff frequency of 1 GHz would then require a hole with a radius of at least 88 mm. A balun designed at this same frequency would have a length of roughly 75 mm,

making the necessary hole significantly larger than the balun itself. Therefore, no significant propagation would occur through any holes in the balun sides. These holes would affect the conductivity of the balun walls, which would only affect the characteristic impedance of the balun, and add a reactance to the characteristic impedance. The effect of this reactance would be the same as the reactance of the short in Section 2.3.2, resulting in shifts in the operating frequency of the balun.

2.3.4 Balun Spacing

In an ideal situation, the opening of the balun would be placed directly at the connection between the coax and the balanced structure, but this is not realizable due to physical constraints. This creates a gap in front of the balun that looks like a length of wire, as can be seen in Fig. 2.4. A length of wire will have a certain inductance, L_{wire}, given by

$$L_{wire} = 0.2w_s(\ln\frac{4w_s}{d} + \frac{d}{2w_s} - 1)[nH], \tag{2.14}$$

where w_s is the length of the wire and d is the diameter [15]. This inductance will have a similar influence as the reactances described in Sections 2.3.2 and 2.3.3 and change the input impedance, Z_{in} in Fig. 2.4, at the point of connection. As this gap increases, so does the inductance. This increased inductance then decreases the fraction of a wavelength needed to reach a large input impedance. This decreased fractional wavelength then results in a lower operational frequency as the same physical length.

2.4 Conclusions

A balun is a type of component necessary for ensuring the proper function of balanced structures and unbalanced structures that are connected, such as dipole antenna and coaxial cable. A common example of a balun is a sleeve balun. When placed on the exterior of coax, a sleeve balun forms a second length of coax with the exterior of the outer conductor of the coax cable. When this length of coax is a quarter wavelength long, it presents a very large impedance to the currents flowing on the exterior of the outer conductor of the cable, known as the common mode. This high impedance forces all of the current to flow on the interior of the of the cable and ensures proper current distributions on the antenna. A measure of this rejection is the Common Mode Rejection Ratio (CMRR) and is a common figure of merit for balun performance.

While the overall length of the balun plays the largest role in determining the operating frequency, other aspects will shift this frequency as well. Any holes or other such imperfections in the shorted end will add a reactance to this load impedance. Visualizing on the Smith Chart, this reactance will shift the starting point slightly off of a true short and will change the electrical length needed to reach an open circuit impedance. As this electrical length changes the physical length cannot change, shifting the frequency at which the opening of the balun presents a large impedance. Likewise, the spacing between the opening of the balun and the connection point of the balanced and unbalanced structures, which is unavoidable in most practical applications, will also lower the operating frequency. The length of wire formed by the exterior of the outer cable conductor will have a certain inductance that varies with length. This inductance will shift the input impedance away from the necessary open circuit impedance. Therefore,

a smaller electrical length is necessary so that the addition of the wire inductance will create a large impedance at the connection point. Again, the physical length is fixed, so the only way to achieve this lower electrical length is to go to a lower operating frequency. Similarly, any holes in the walls of the balun will shift the operating frequency. The holes add a reactive component to the characteristic impedance of the balun, which will have the same affect as a reactance in the shorted load impedance. The diameter of the pipe forming the balun also affects the characteristic impedance, adding another reactive component that will have a similar effect.

Chapter 3

Additive Manufacturing

Additive manufacturing has grown significantly in popularity as higher quality methods have become more cost effective, allowing for their more widespread use both commercially and industrially. As was discussed in Chapter 1, additive manufacturing is the process of created a final component by adding material, as opposed to removing material in subtractive processes. This process allows for significantly greater geometric complexity compared to other methods, allowing for the creation of structures that would be incredibly difficult otherwise. This is a large benefit that has caused additive manufacturing to be applied to many different areas.

The most commonly known form of additive manufacturing is known as 3D printing. There are several types of 3D printing widely available, each with its own advantages and disadvantages. The most widely used is Fused Deposition Modelling (FDM), which constructs a component by extruding a melted polymer out of a nozzle in a line to form layers. The main benefits of FDM are low equipment and material costs. It does not have as high of print quality as other methods,

however. Another type of 3D printing is stereolithography (SLA) which utilizes an ultraviolet laser to selectively cure an ultraviolet-sensitive resin, constructing a component layer by layer. This type of printing gives significantly higher resolution prints compared to other methods with up to 25 $\mu\ m$ of resolution because it only depends on the fidelity of a laser point, as opposed to fluid flow out of a nozzle in FDM. Another benefit of SLA printing is that since each layer is create almost instantaneously it is possible to create more significant unsupported overhangs than other methods without the risk of deformation. The downside to SLA is that the equipment and materials are more expensive than other methods. The final commonly discussed form of 3D printing is selective laser sintering (SLS), which uses an intense laser to selectively melt metal powder in layers to construct a component. This method has the benefit of producing a fully metallic component with no further processing, but the equipment needed for this process is very expensive and is therefore not widely available.

3.1 Additive Manufacturing in RF & Microwave Applications

Additive manufacturing has also been applied to RF and microwave applications [16–20]. For example, it has been used to create a plastic or resin component that is then given some amount of conductivity through the use of conductive paints and epoxies or electroplating [16, 19, 20]. Furthermore, SLS has been used to directly create Rf components such as waveguides [17, 18]. From these it can be seen that additive manufacturing is a large area of active research with much that can still be done.

3.2 Conclusions

In conclusion, additive manufacturing is a method of producing a component by selectively adding material, usually in layers. There are several different types of additive manufacturing processes available, each with its own advantages and disadvantages. For example, FDM has low equipment and material costs, however it also has lower resolution than other methods. Another type, SLA, has significantly higher resolution at up to 25 $\mu\, m$, but both materials and equipment are more expensive. Finally, SLS offers the capability of directly producing fully metal components, but the machinery is significantly more expensive than other methods and is not widely available. All of these methods have, however, been studied and established for use in RF and microwave applications, opening the door to many future possiblities.

Chapter 4

Traditional VS Printed Sleeve Baluns

As mentioned previously, sleeve baluns have many issues, some of which being weight and manufacturing requirements. A balun constructed out of a copper pipe would be heavy, difficult to solder with just a soldering iron as any heat would be immediately dissipated, and would take a significant amount of time to make a single one. A 3D printed balun would not have these issues. Materials used in 3D printing are significantly lighter, could be assembled without the use of any heated equipment, and can be manufactured in batches so the time to make multiple baluns is only marginally longer than the time to make one. There are, however, other aspects, such as supporting structures and fluid flow, that need to be considered and accommodated.

In order to assess the feasibility of 3D printed baluns, a balun matching the design of a traditional balun was printed using a Formlabs Form2 © stereolithography (SLA) printer, which was chosen for its high print resolution at 25 microns [21]

and other benefits of SLA printers over other types, which will be described and utilized in Section 5.2. These baluns cannot function as baluns immediately after printing, however, because material used by the printer is a low conductivity resin. Thus, the baluns must be metalized in some way in order to become functioning RF components. The chosen method of metalization was a combination of electroless plating and electroplating. Prior to plating, the balun was put onto a length of semi-rigid coax and fixed in place using a quick curing epoxy. Once the epoxy fully cured, the balun was then first electrolessly plated to form a nanometers-thick layer of copper using the Copper-4000 Electroless Plating process [22]. The balun was then plated with a 600 μin layer of copper using traditional electroplating methods. This method of affixing the unplated component to the coax and then plating ensures a high quality seem at the point of connection with little chance of lumps or cracks. A similar method where the balun was plated and then secured to the coax using a conductive epoxy was also tested. This method ultimately did not yield as consistent results. The process of inserting the coax into the balun can cause the plated copper to crack and flake and attempting to create a good connection using the conductive epoxy by hand is a messy process and can result in unwanted lumps on the interior of the balun, which would affect the performance. The quick curing epoxy was both cheaper and gave very consistent quality results.

The baluns, seen in Fig. 4.1, were designed to operate at 915 MHz. The diameter of the printed balun was chosen based on dimensions of commonly available copper pipe, but it does not have a large impact on the performance of the balun, as shown in Section 2.3.3. In order to ensure complete coverage of the plated copper, the traditional balun had to be modified slightly. The hole seen towards the base of the balun in Fig. 4.1(b), which is mirrored on the other side of the

balun, was added to ensure proper flow of plating solution throughout the entire balun. Without these holes or ones similar to them there would be areas of stagnant fluid, resulting in uneven or incomplete plating. This incomplete plating would affect the performance of the balun drastically, shifting the operating frequency unpredictably, and makes the easily characterized frequency shift associated with the holes the clear choice. The extreme extension of this is the balun in Fig. 5.13(a), where the entire body of the balun is filled with holes to absolutely ensure complete plating. Even at this extreme, the holes only add a reactive value to the characteristic impedance of the coax and, as shown in Section 2.3.3, cause a frequency shift that can easily be accounted for. The exact sizing of these hole is a matter of balancing plating quality and structural integrity. If they are too large the balun will be very fragile and if they too small they might close in the printing process and not allow fluid through.

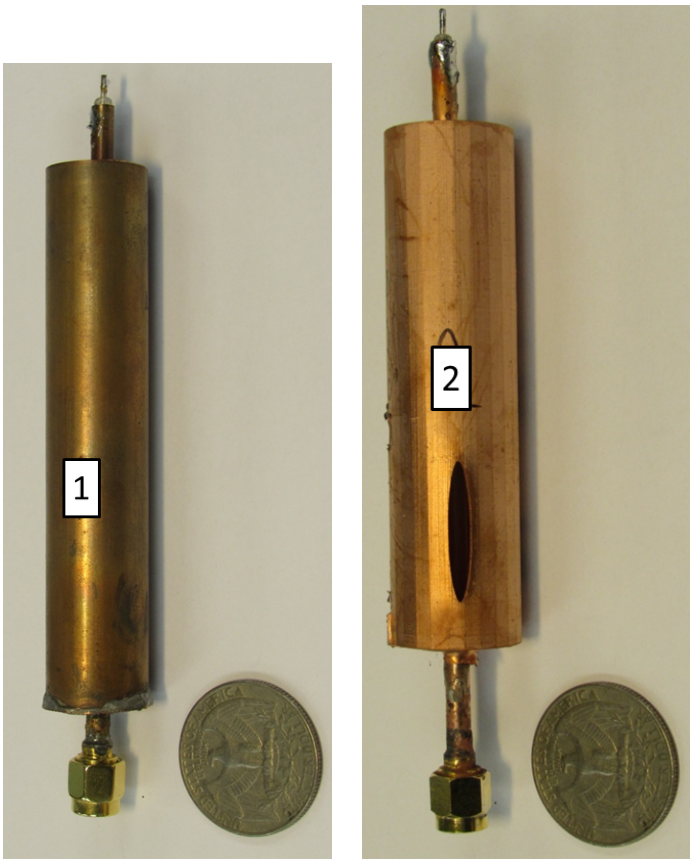

(a) (b)

FIGURE 4.1: A comparison of a traditionally manufactured unfolded sleeve balun (a) and an additively manufactured, electroplated unfolded sleeve balun (b), both with a standard American 25¢ coin for reference.

4.1 Measurements

4.1.1 CMRR

Both baluns in Fig. 4.1 were connected to a network analyzer, in the same configuration as the balun in Fig. 2.2, and the CMRR and Insertion Loss were measured. A comparison of these measurements can be seen in Fig. 4.2.

These results show a minor difference in the operational frequency of the first

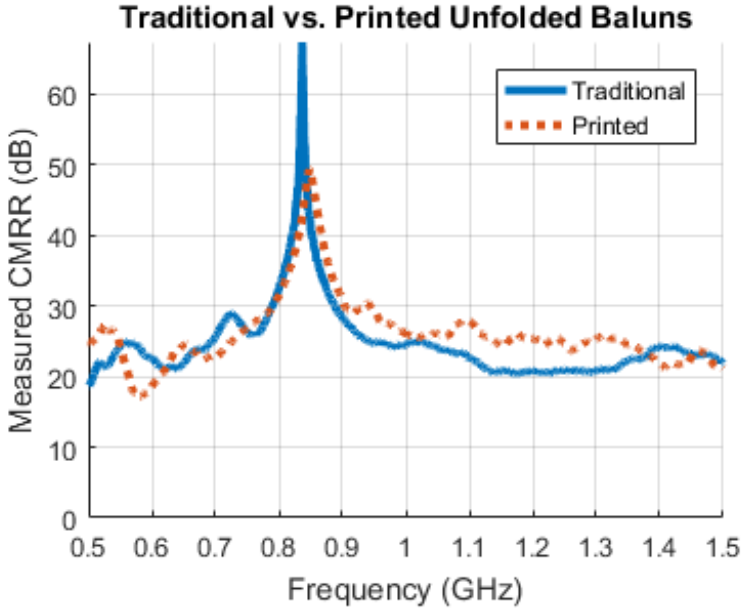

(a)

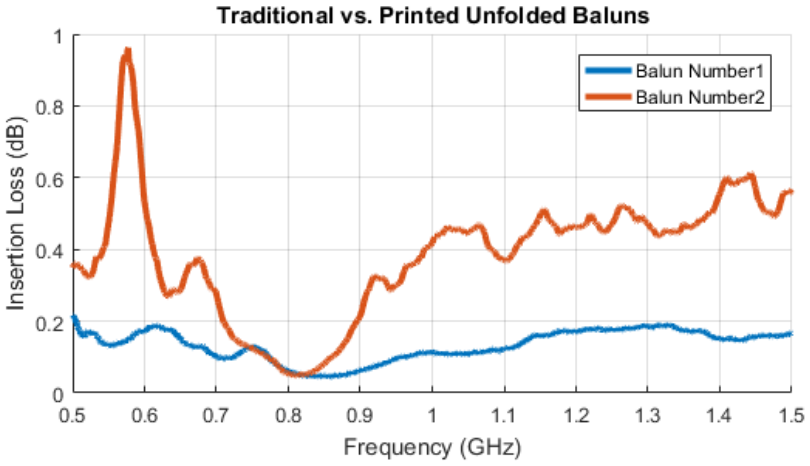

(b)

FIGURE 4.2: A comparison of the CMRR of a traditionally manufactured unfolded sleeve balun and an additively manufactured unfolded sleeve balun (a) and the insertion loss of the two baluns (b).

two baluns and a difference in the level of rejection between the two. The frequency shift comes from the slight difference in overall length that resulted from inaccuracies in the method used to cut the pipe. The decreased rejection would amount to very slight variations in the attachment of the twinlead on the differential probe jig to the semi-rigid coax. Inserting the peak values of CMRR for the copper pipe balun and the printed, unfolded balun, which are 67.3 dB and 49.3 dB respectively, into Equation 2.1 and solving for the ratio of S_{21} to S_{31}, it can be found that the ratio is 1.00087 for the copper pipe balun and 1.00688 for the printed, unfolded balun. Therefore, this difference in CMRR amounts to a 0.601% difference in the ratio of S_{21} to S_{31} in these two baluns, which can easily occur when connecting components by hand.

4.1.2 Dipole Radiation Patterns

In order to fully test the performance of the baluns in an actual application, a dipole with a resonant frequency matching the operating frequency of the each balun in Fig. 4.1 was connected to each balun and the realized gain was measured in two cut planes, the H-plane when the dipole is vertical to the ground and the E-plane when it is horizontal to the ground. As has been stated previously, a dipole is a balanced structure, therefore if the balun is adequately choking the common mode current on the coax, then the dipole should function properly and give a characteristic dipole radiation patter, as shown in Fig. 4.3.

As can be seen in Fig. 4.4, the presence of the balun at this frequency ensures a smoother, more circular pattern in the H-plane measurements and deeper nulls in the E-plane measurements. Slight variations from the ideal dipole pattern, such as those in Fig. 4.5, can occur due to human error in the placement of the

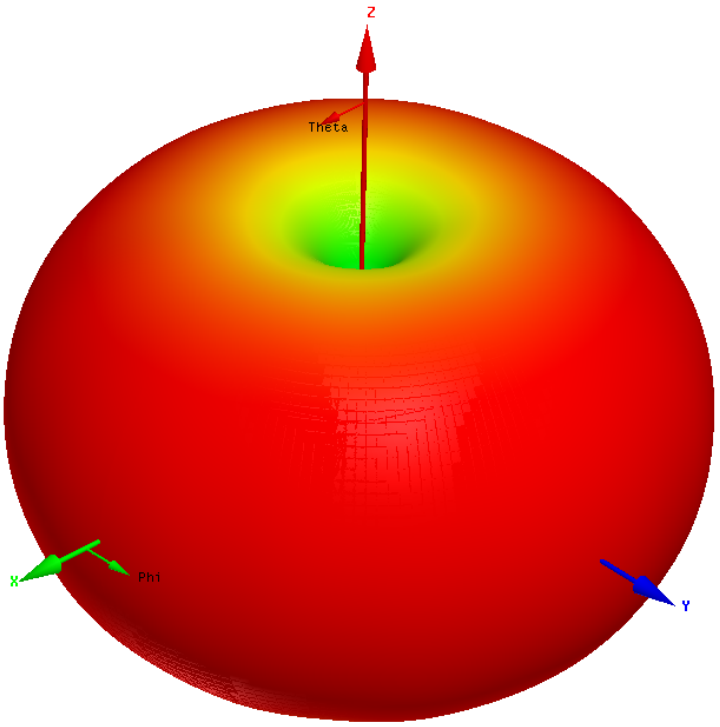

FIGURE 4.3: The ideal dipole radiation pattern of a dipole directed along the Z axis.

dipole. Any difference between the center of the dipole and the center of rotation will result in a similarly shifted pattern.

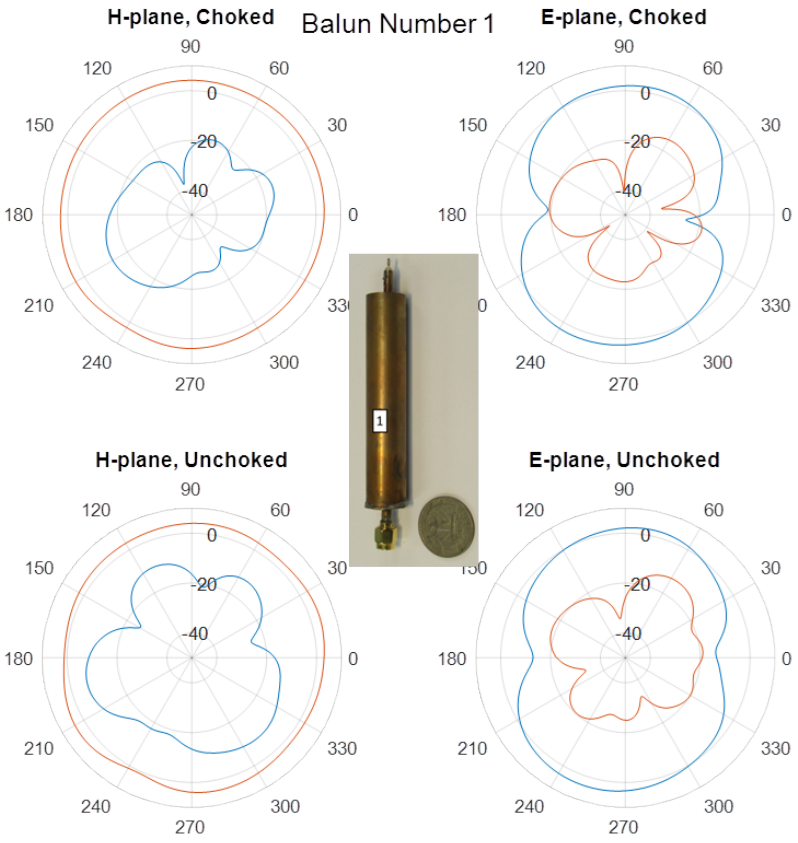

FIGURE 4.4: The measured radiation pattern of a dipole connected to a copper pipe unfolded balun at its operating frequency (top) and the measured radiation pattern of a dipole with no balun at the same frequency (bottom).

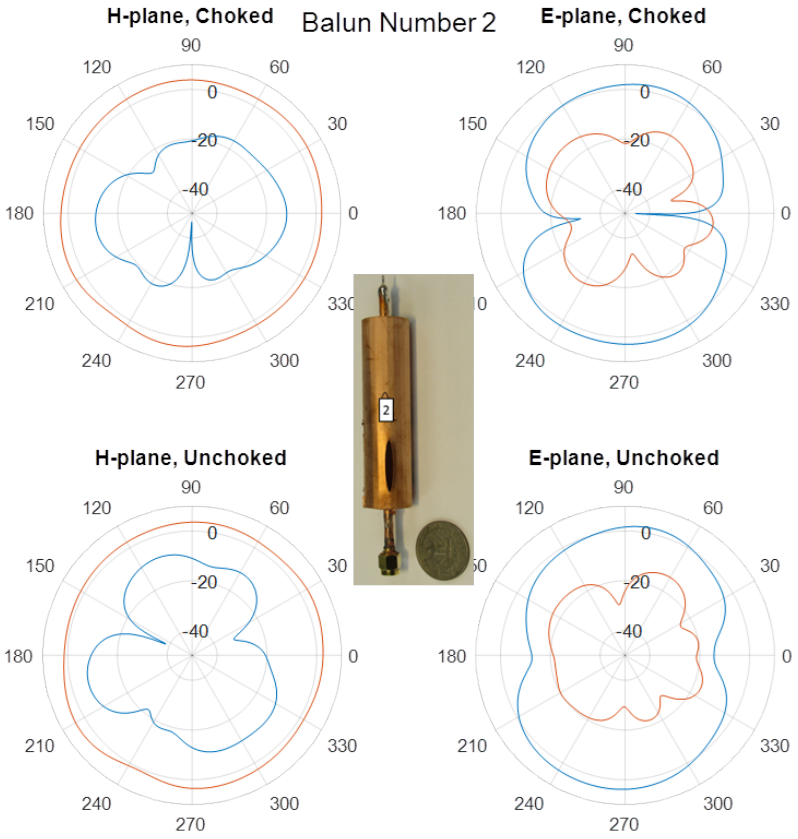

FIGURE 4.5: The measured radiation pattern of a dipole connected to a printed unfolded balun at its operating frequency (top) and the measured radiation pattern of a dipole with no balun at the same frequency (bottom).

4.2 Conclusions

Sleeve baluns can be constructed using additive manufacturing techniques to eliminate some of the disadvantages of these baluns, such as weight and production requirements. To test the feasibility of 3D printed baluns, a balun was printed to match the design of a traditionally manufactured balun. The balun was printed and plated with copper and both baluns, printed and traditional, were tested. As can be seen in Fig. 4.2, there is a minor frequency shift due to imprecision in the cutting process of the traditional balun. The overall rejection is also lower for the printed balun due to increased surface roughness compared to the copper pipe balun, but it is still above 38 dB and is therefore still a well functioning balun. This difference in CMRR can be attributed to human error, as any slight difference can create a large difference in CMRR above 38 dB. The baluns were also tested by attaching a dipole and measuring the realized gain. As can be seen in Figures 4.4 and 4.5, the baluns do ensure proper functioning of the dipoles at their operating frequency.

Chapter 5

Folded Baluns

5.1 Introduction

One of the largest detriment of sleeve baluns is their size. Ferrite beads are a common alternative to sleeve baluns for choking cable currents because they offer a small form factor, however they are only effective up to roughly 100-200 MHz [10]. Above this frequency, sleeve baluns are a viable option. At these frequencies, however, a sleeve balun can be on the order of tens of centimeters long, given that it must be a quarter wavelength long. This places significant space requirements that remove it as an option for many applications. This has created an interest in various means of reducing these size requirements.

An established method of reducing the size of a sleeve balun is by folding it [5, 6]. As can be seen in the cross-section in Fig. 5.1, a second length of coax is created within the same overall diameter. Since the effective length has roughly doubled with the addition of the second coax, the balun can be shrunk by roughly

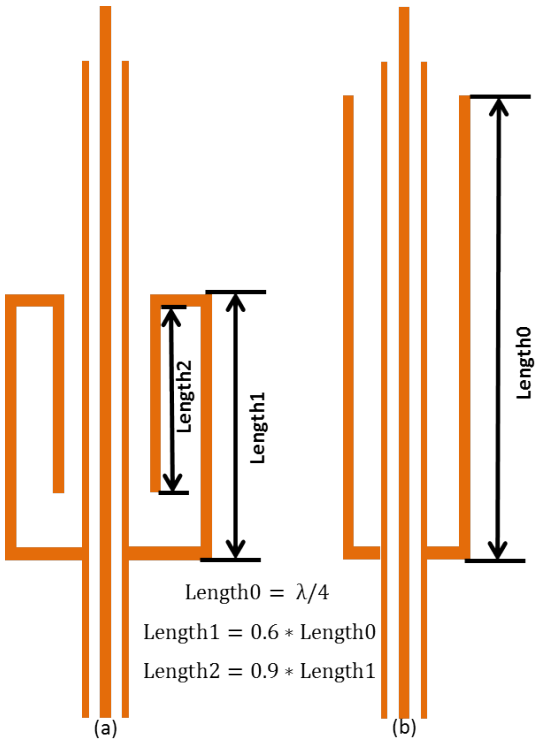

FIGURE 5.1: The illustrated cross sections of a balun folded a single time (left) and an unfolded balun (right).

half, with the exact size reduction and ratios being tuned to maintain the same operating frequency.

These folded baluns are still composed of all the same aspects as the ones discussed in Section 2.3, but one additional aspect is added, the corner section between the two lengths of coax. In order to extract the behavior characteristics of this corner section, the structure in Fig. 5.2 was simulated using ANSYS High Frequency Structure Simulator [12]. The structure is a folded balun that is open at both ends with waveports placed at the openings. Using this simulation, the scattering parameters can be simulated. These results can then be used to de-embed the characteristics of the corner, which can be seen in Fig. 5.3. As can be seen by these results, the corner section simply acts as a thru between the two lengths of coax and does not have a significant effect on the performance,

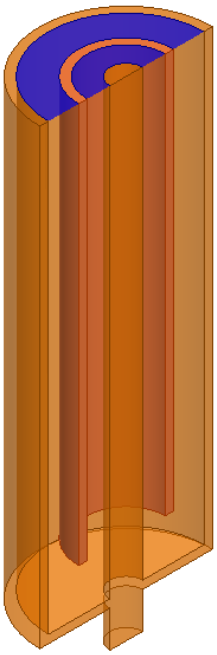

FIGURE 5.2: The cross section of the lengths of concentric coax simulated using HFSS in order to extract the characteristics of the corner section. The dark blue sections are the waveports.

especially at low frequencies.

Although these folded baluns do offer equitable performance to traditional sleeve baluns in a smaller package, they do not offer a fabrication benefits when constructed using traditional methods. There are now twice as many points as an unfolded balun that must be welded together and applying the necessary heat to weld any one of them can lead to others coming apart. Additionally, these folded baluns cannot be tuned once they are fully constructed as the process of de-welding one part and re-welding everything together would have a greater impact on the operating frequency than shortening one length of pipe. These difficulties are then compounded for greater than a single fold, leaving multi-folded baluns all but completely unexplored. However, the freedom gained by utilizing additive manufacturing does allow for the creation of novel multi-folded baluns.

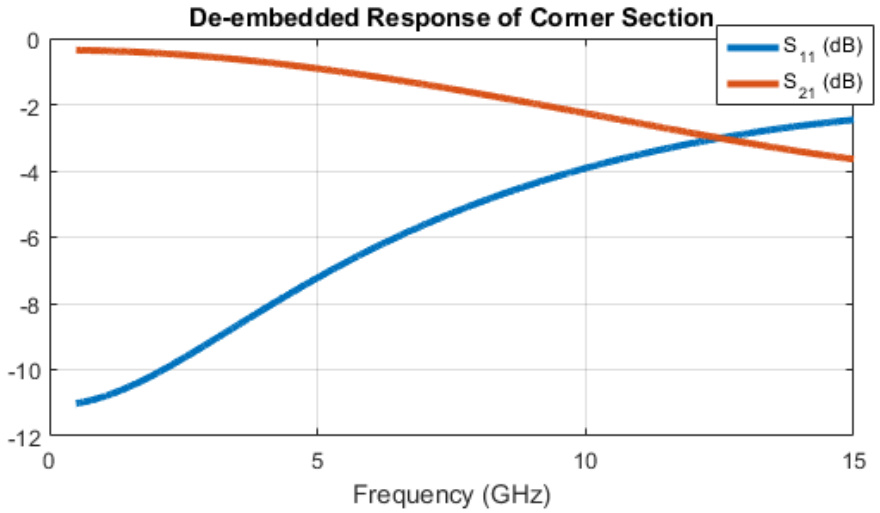

FIGURE 5.3: The de-embedded scattering parameters of the corner section found by moving the measurement plane to the openings of the cavity.

5.2 Design & Fabrication

5.2.1 Single Folded Baluns

While additive manufacturing does not share the same limitations as traditional methods and can create things that would be prohibitively difficult or outright impossible otherwise, it does have its own set of constraints. A primary constraint is orientation and unsupported structures, or structures that would not be connected to the main body of the print when they begin printing. A component such as the one illustrated in Fig. 5.4 would not print properly because the unsupported center section would remain unconnected to the rest of the print until the very end. However, as soon as the printer would start on this section, the material would fall away or get in the way of the printing mechanism causing the rest of the print to fail. One remedy for this issue is the use of supports, which are small structures that are designed to support sections of the print and ensure print quality and then break away easily. Many programs designed for

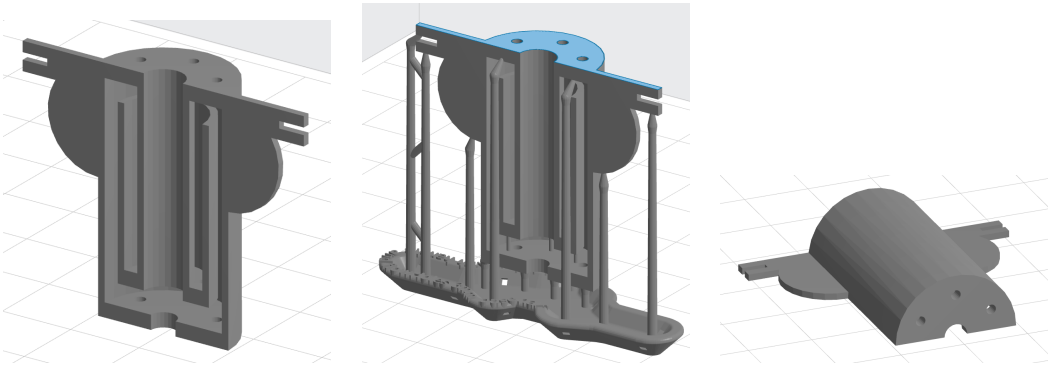

(a) (b) (c)

FIGURE 5.4: An example of a structure that would fail to print properly (a), the same structure with supports that 3D printing software, such as Preform©, in this case, can generate automatically (b), and the same structure reoriented to print without the need for supports (c).

generating print files, known as slicers because they slice a model into layers that a 3D printer can easily print, can generate supports automatically, such as in Preform© in Fig. 5.4 [23]. Another remedy for unsupported structures is making use of different orientations that might exploit certain aspects of a printer. For example, the same structure in Fig. 5.4 would be printable without the use of supports if it is simply flipped vertically. By doing this, there are no unsupported areas until the outer cylinder is closed at the top. Some printer types would not be able to print the top of this cylinder without any errors, but a stereolithography (SLA) printer, such as the Formlabs Form 2 ©, is able to do this without issue because each single layer is created almost instantaneously, removing any time for the area to fall or sag.

Using a Formlabs Form 2 ©, the folded balun in Fig. 5.5 were printed monolithically, or in completely one piece, such that no support structures were necessary.

To assemble, a length of semi-rigid coax was fed through the hole in each of the baluns and secured in place using a quick-curing epoxy. After curing according to

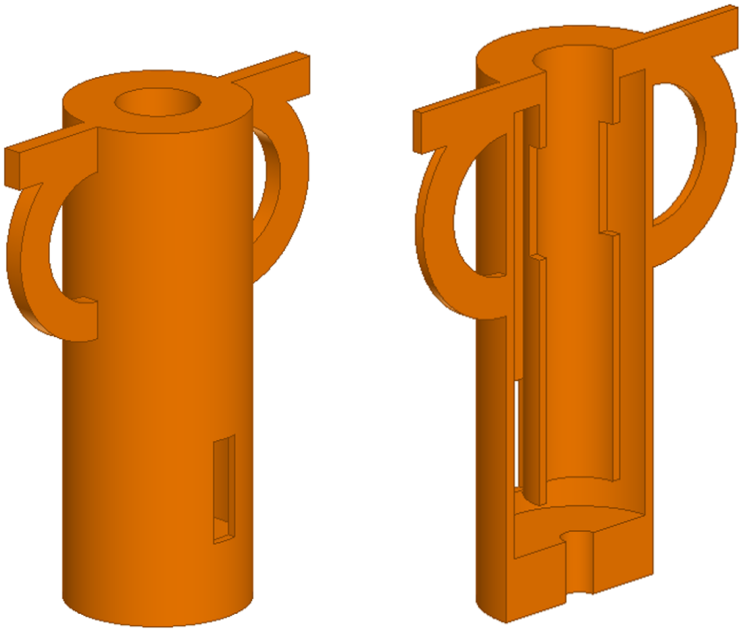

(a) (b)

FIGURE 5.5: The print model of a single folded balun (a) and its cross-section (b).

the manufacturer instruction, the baluns were plated following the same process used for the unfolded in Section 4. The final plated baluns can be seen in Fig. 5.6.

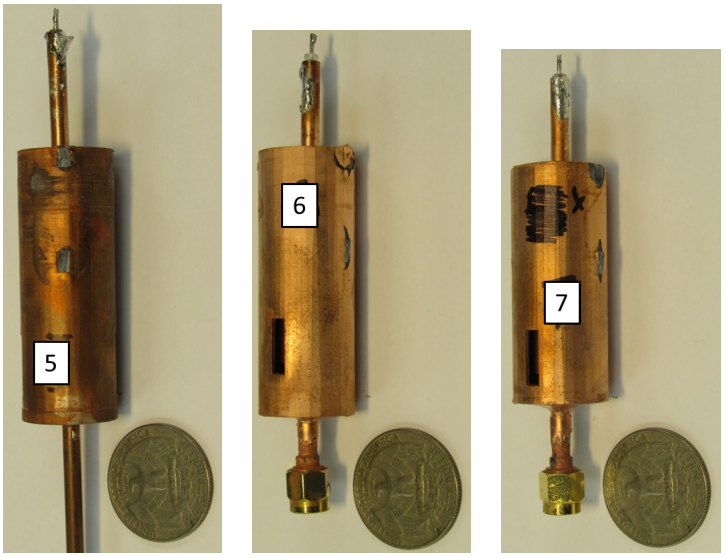

(a) (b) (c)

FIGURE 5.6: The final assembled single folded baluns, all with a standard American 25¢ coin for reference.

5.2.2 Double Folded Baluns

While the unfolded and single folded baluns could be printed monolithically with no supports, that is not possible for baluns folded a greater number of times. As illustrated in Fig. 5.7, it is not possible to print this balun in such a way that the second wall from the exterior, labeled Wall 2, is connected to the rest of the print. It is for this purpose that a new design was developed.

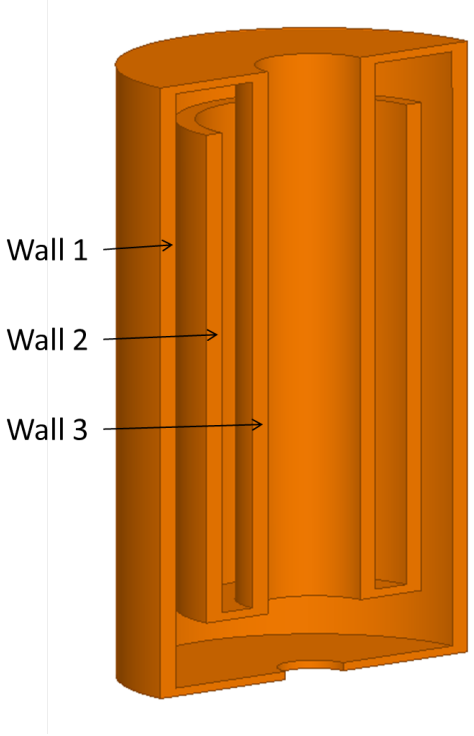

FIGURE 5.7: The cross-section of a double folded balun with its walls numbered.

5.2.3 Improving Print Quality

The simplest method of improving the printability, or ease of which something can be printed, is to slice the balun in half across its diameter and print each half with the new opening facing the print surface. This is not a complete solution, however, because parts printed like this are to prone breaking in the removal process and are difficult to properly align when assembled. The first attempt to remedy this was to add two sections on either side that would act as registers in the final assembly and use supports. As can be seen in Fig. 5.8, the spaces between the points where the supports connected to the face of the balun sagged and shifted in the printing process, resulting in a rough surface that would not allow for proper assembly. In response to this, ridges, seen in Fig. 5.9, were added along the joining surface that serve dual purposes. They improve print

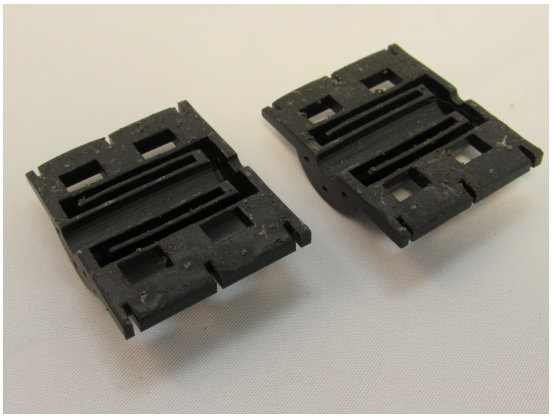

FIGURE 5.8: A poorly printed double folded balun.

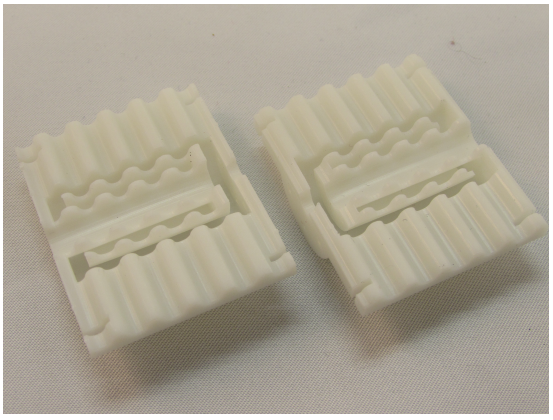

FIGURE 5.9: The newly designed balun with ridges that improve print quality and act as registers between the two halves.

quality because the supports can be added at the minima of the ridges, thus supporting the print more efficiently by making use of the structural qualities of arches and allowing for the easy removal of the supports without impacting the rest of the print. The ridges also act as registers between the two halves in the assembly process and allow for the halves to snap and hold onto the semi-rigid coax.

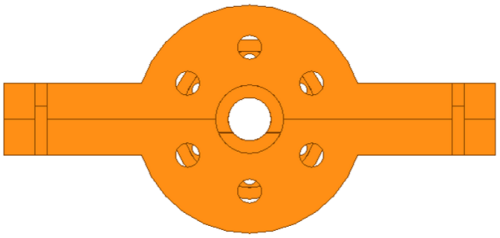

FIGURE 5.10: This top view shows how there are completely clear paths for the electroplating solution to flow all the way through the double folded balun with holes in the top and bottom faces.

5.2.4 Improving Plating Quality

Utilizing this new print design, the first design of a double folded balun was printed, which can be seen in Fig. 5.9. This design is the double folded analog of the single folded baluns in Fig. 5.6(a)-5.6(c), where the walls are kept largely solid but a few holes are added to promote adequate fluid flow. The primary difference between these designs is that the fluid flow holes were moved to the flat faces of the cylinders as opposed to on the walls in the single folded baluns. This was done to allow for complete, unimpeded paths for the fluid to flow through the balun, which can be seen in the top view in Fig. 5.10 by the fact that one can see all the way through from one end to the other. The effects of these holes follows the principles laid out in Section 2.3.2.

The unplated resin halves were then secured to a length of semi-rigid coax and plated using the same methods and processes as the unfolded baluns in Section 4 and single folded baluns in 5.2.1. A double folded balun constructed using this method can be seen in Fig. 5.11(b). This method gave some functioning plating results, but it did not give consistently complete plating throughout the

interior. To improve these results, other designs and methods of assembly were investigated.

The first alternative was designed to improve the plating quality of the existing double folded balun design. As opposed to plating the entire assembly after the printed halves had been adhered to the semi-rigid coax, the printed halves were instead plated individually. Having the faces completely open like this allows for the plating fluid to flow fully around the walls of the halves and completely cover the parts in an adequately thick layer of copper. These plated parts can then be attached to any existing cable, provided it is the proper radius for which the baluns were designed. The snapping effect from the registers added in Section 5.2.3 creates a strong enough electrical connection that the balun can operate with no additional adhesive or clamp. This then allows for the exact operating frequency of the balun to be tuned by shifting the location of the balun up or down the length of the semi-rigid coax, changing the inductance discussed in Section 2.3.4 by changing the length the wire formed by the exterior of the outer conductor of the coax. Once the desired operating frequency is achieved, the plated halves may be secured in place using any standard form of adhesive. A further extension of this can be seen in Fig. 5.12. Here, a double folded balun was printed and plated in four separate pieces, seen in the exploded view in Fig. 5.12(a), that were then assembled to get the final balun in Fig. 5.12(b). The interior dimensions of this balun are the same as the previous double folded baluns, however the exterior walls were thickened in order to provide more structural integrity for the connecting posts, visible on the lower two segments in Fig. 5.12(a).

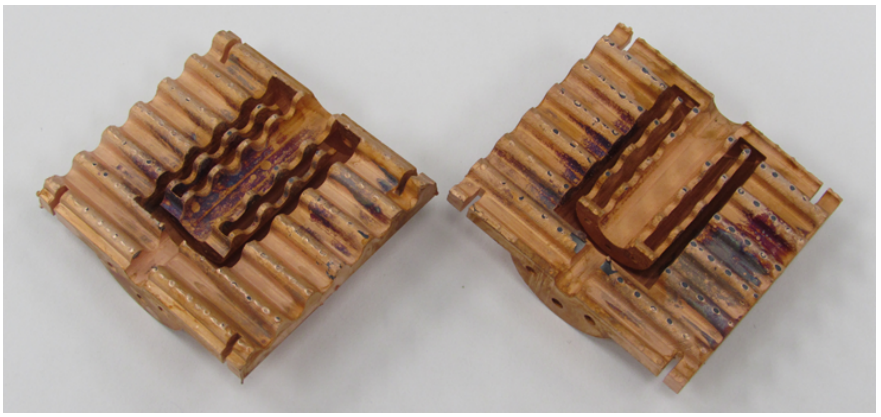

(a)

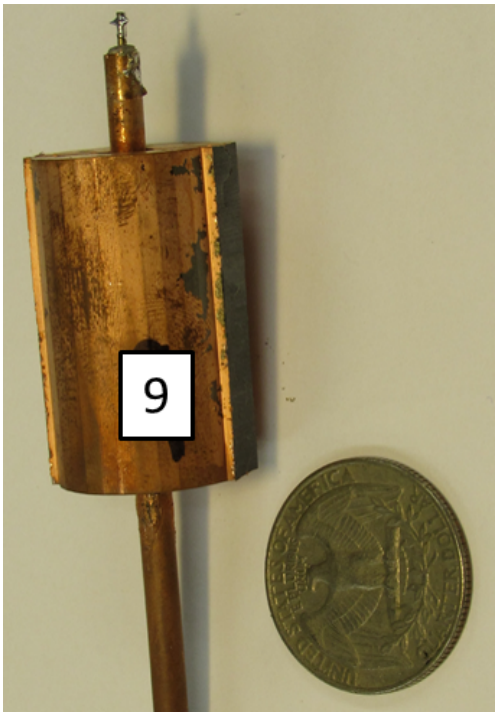

(b)

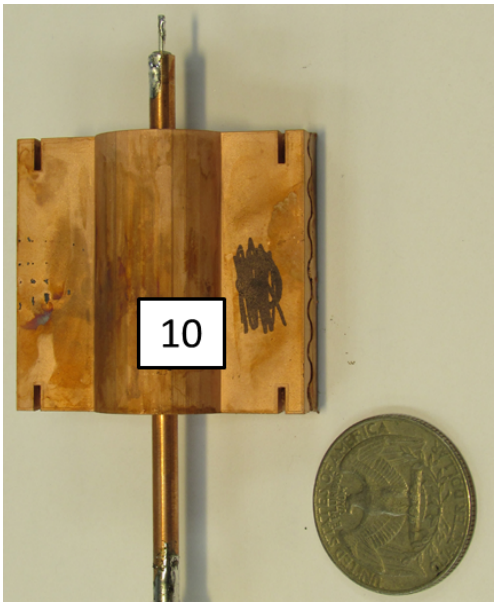

(c)

FIGURE 5.11: Examples of two plated halves of a double folded balun (a), a balun that was plated after the two halves are attached to a length of coax (b), and a balun that was plated before the halves were attached, with a standard American 25¢ coin for reference in (b) and (c).

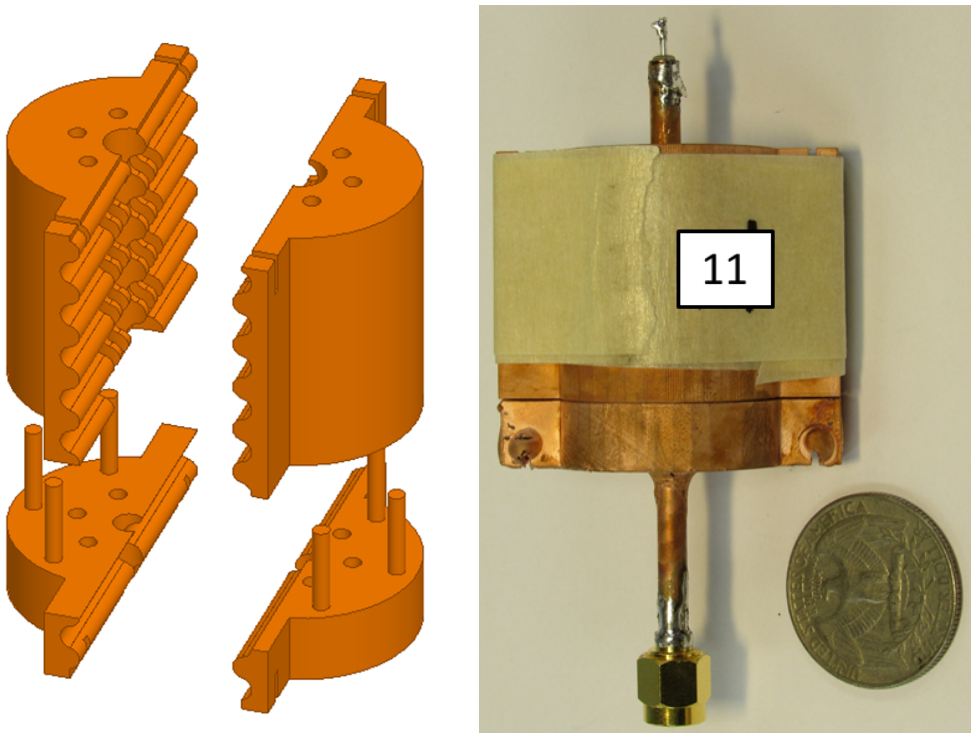

(a) (b)

FIGURE 5.12: An exploded model showing the individual parts of a segmented, double folded balun (a) and a final, assembled segmented double folded balun (b) with a standard American 25¢ coin for reference.

5.2.5 Mesh Baluns

The second alternative was the mesh balun designs seen in Fig. 5.13. The walls of these baluns were designed to maximize the flow of fluid throughout the interior. Even though the previous designs for unfolded and single folded baluns performed adequately and consistently, unfolded and single folded baluns were constructed with mesh walls in order to verify the performance of the design.

Once the mesh wall design was confirmed, it was then applied to the double folded balun design, resulting in the baluns found in Fig. 5.14. All of these mesh baluns were attached to lengths of semi-rigid coax and plated using the same methods as in Sections 4 and 5.2.1 for the unfolded and single folded baluns.

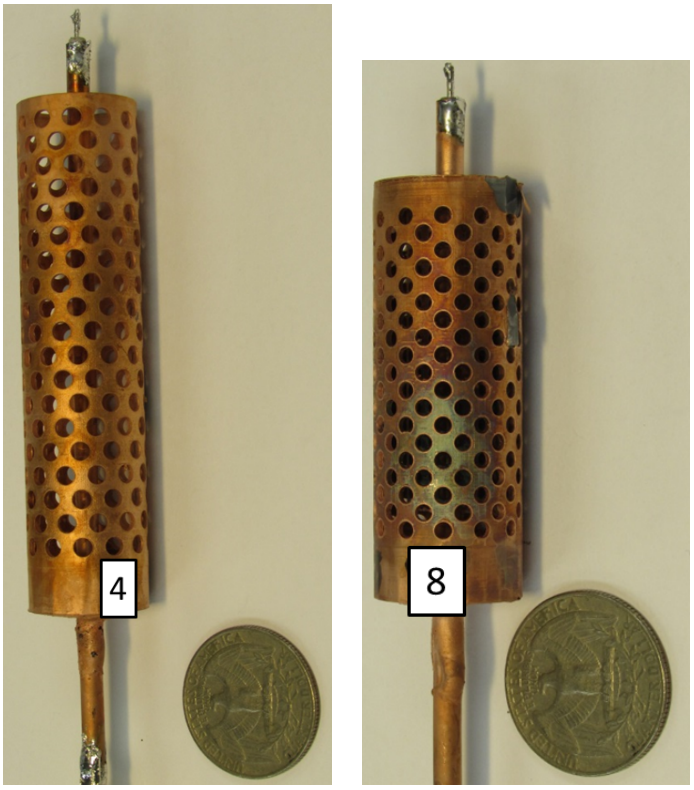

(a) (b)

FIGURE 5.13: The baluns designed and tested using the mesh wall design, which was designed to maximize fluid flow throughout the interior. The balun in 5.13(a) is an unfolded balun and the balun in 5.13(b) is a single folded balun

The double folded baluns were both plated after being attached and before as in Sections 5.2.2 and 5.2.4, respectively.

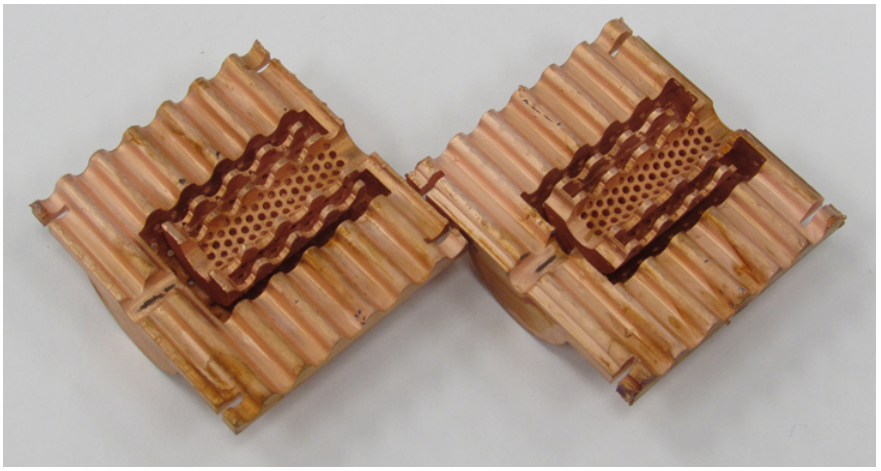

(a)

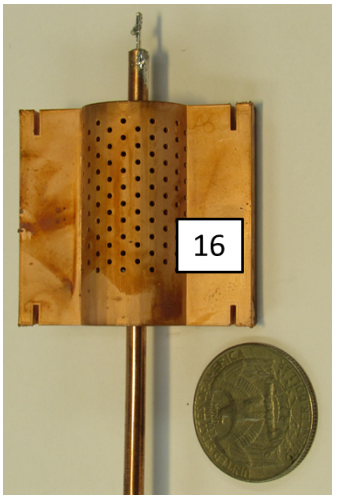

(b)

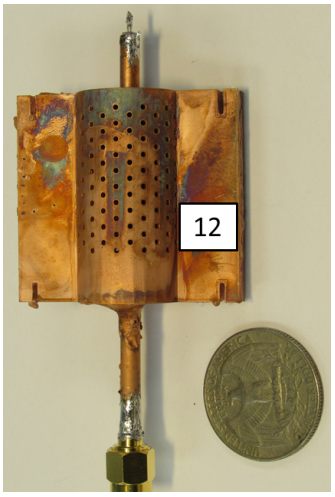

(c)

FIGURE 5.14: The two plated halves of a mesh double folded balun (a) and two mesh double folded baluns that were either plated before being attached (b) or after being attached (c), with a standard American 25¢ coin for reference.

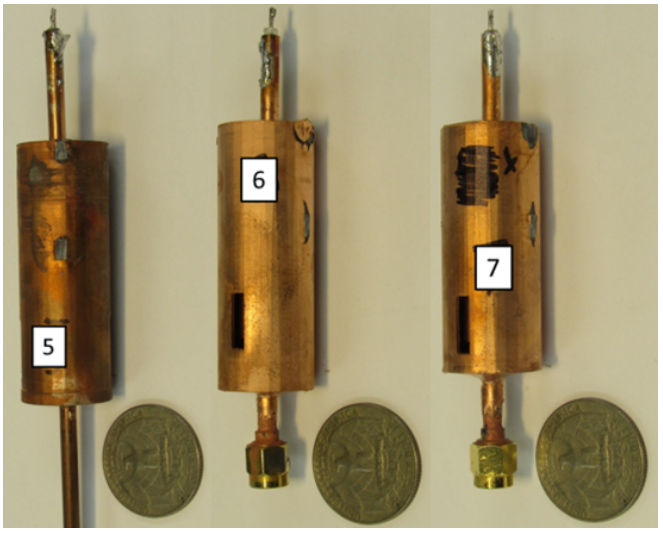

FIGURE 5.15: The printed single folded baluns from Section 5.2.1

5.3 Measurements

5.3.1 CMRR

All of the plated baluns discussed in Section 5.2 were tested using the same method as was used in Section 4.1. The 3-port network parameters were measured using the differential probe jig seen in Fig. 2.2 and the CMRR was extracted from these measurements using Equation 2.1. The Insertion Loss was also calculated as done in Section 2. The results for the single folded baluns in Section 5.2.1 can be seen in Fig. 5.16. The results for the double folded baluns in Section 5.2.2 can be seen in Fig. 5.18. The tuning capabilities of the changing the placement of the balun along the length of the coax was also tested using the solid-walled and mesh double folded snap-on baluns from Section 5.2.4, with the results shown in Fig. 5.21.

As can be seen in Fig. 5.16, the baluns all have greater than 38 dB of rejection at

their operating frequency, which confirms the validity of using additive manufacturing to create baluns that are prohibitively difficult to manufacture otherwise. The double folded baluns in Fig. 5.18 show similar levels of rejection for those designs. The mesh baluns, whose results can be seen in Fig. 5.20, also achieved greater than 38 dB of rejection. The placement of the double folded mesh snap-on balun was also varied, giving the results in Fig. 5.21. These results show that the operating frequency of the balun does indeed decrease as the space between the opening of the balun and the connection point of the twin-lead increases, as was shown in Section 2.3.4, with a tuning range of 70 MHz.

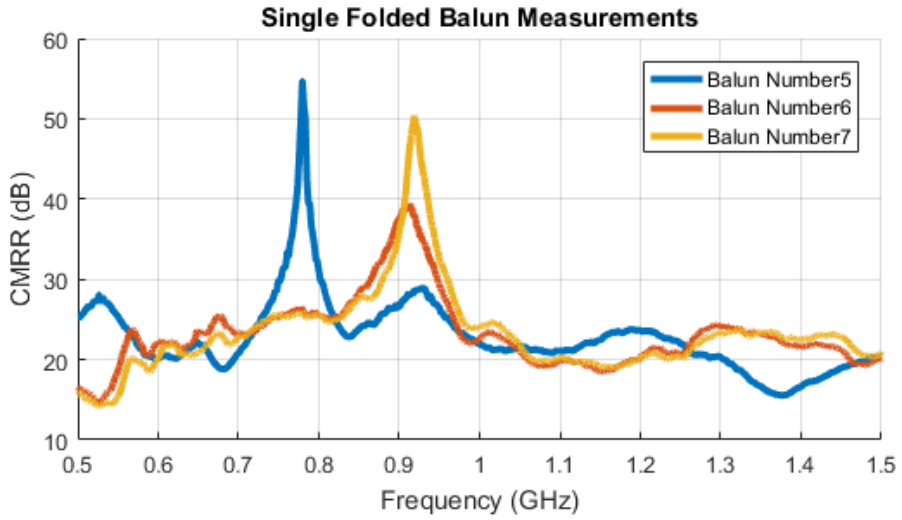

(a)

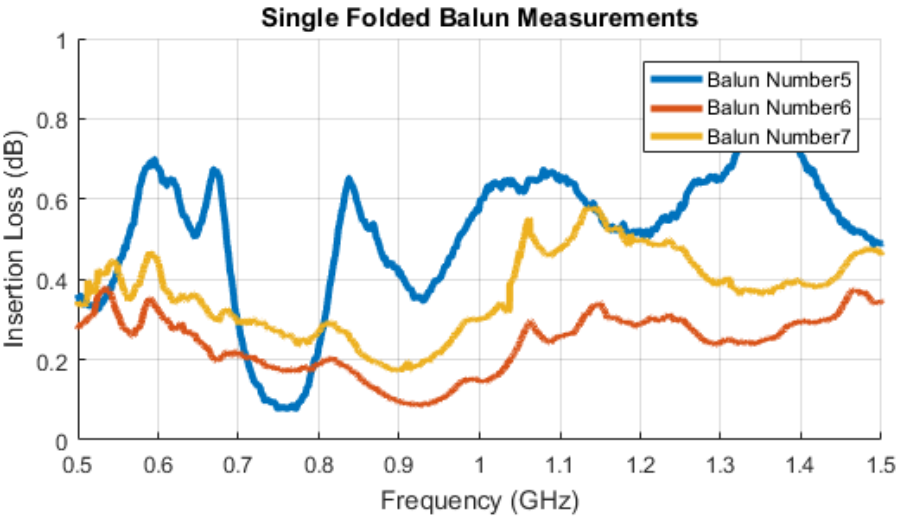

(b)

FIGURE 5.16: The measured CMRR data (a) and the measured Insertion Loss (b) of the balun in Fig. 5.15.

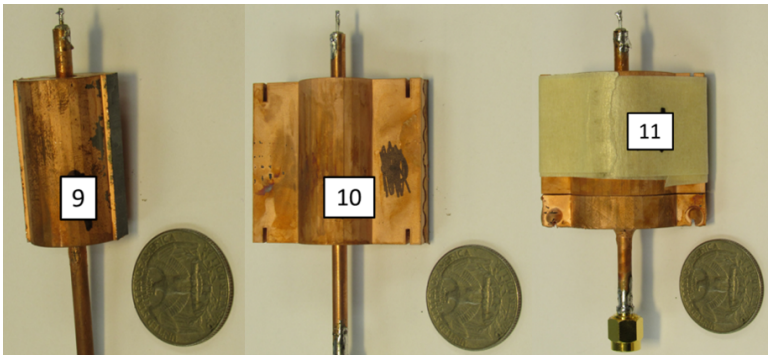

FIGURE 5.17: The printed double folded baluns from Section 5.2.2.

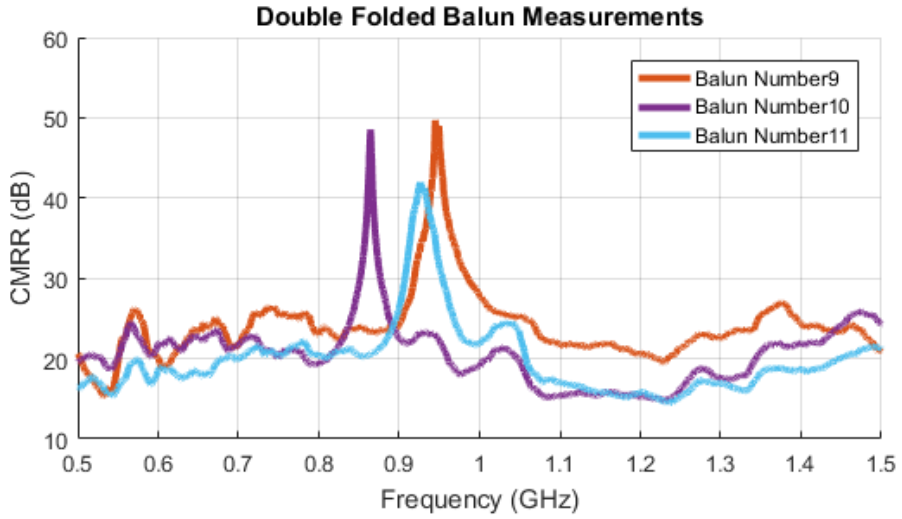

(a)

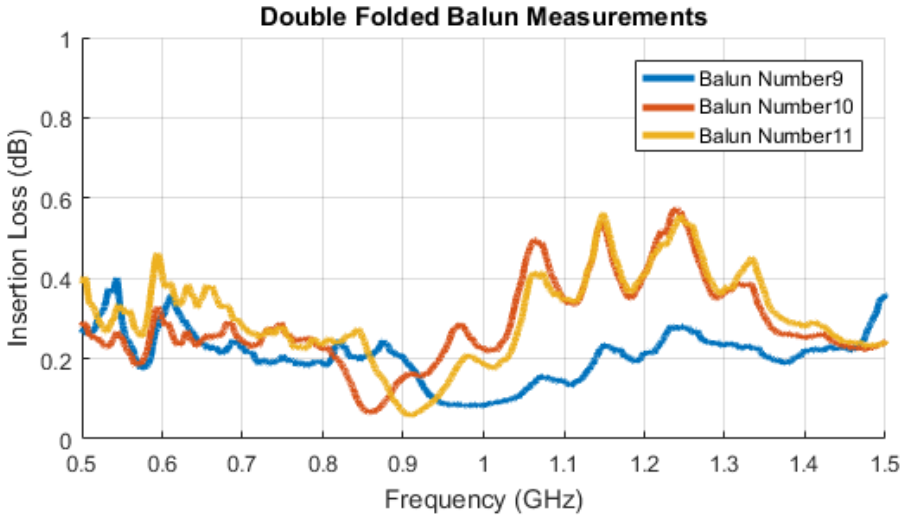

(b)

FIGURE 5.18: The measured CMRR data (a) and the Insertion Loss (b) of the baluns in Fig. 5.17.

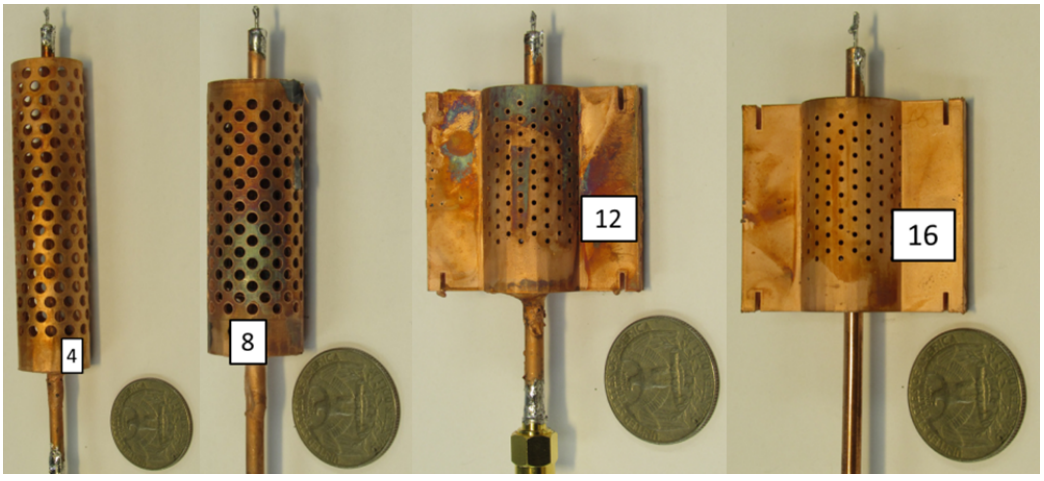

FIGURE 5.19: The final printed mesh baluns from left to right: An unfolded balun, a single folded balun, a double folded balun, and a double folded snap-on balun.

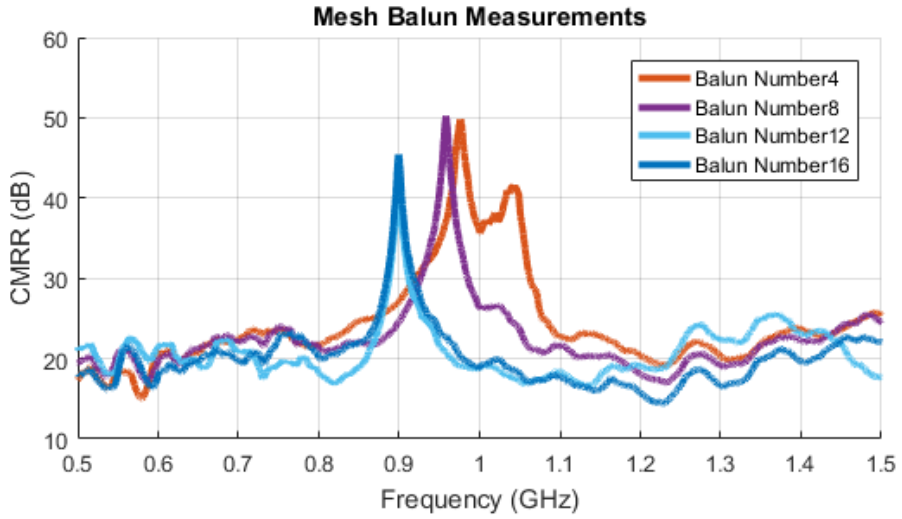

(a)

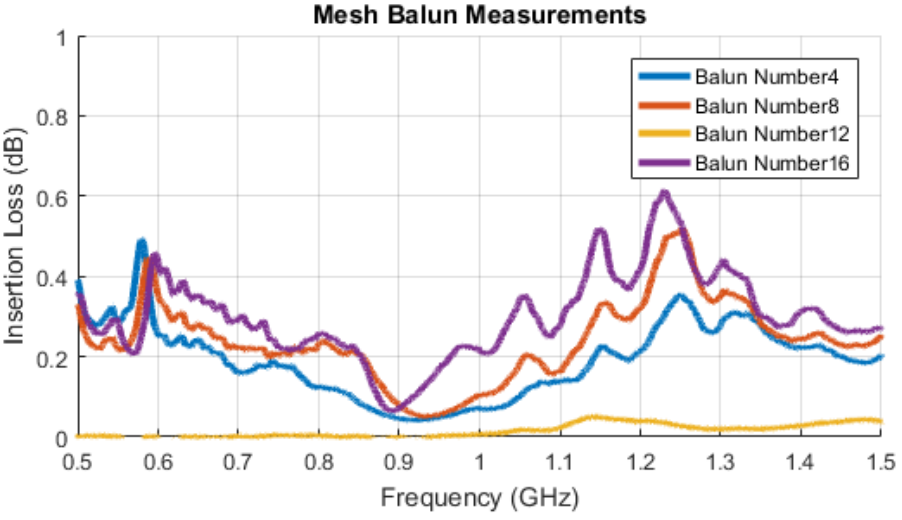

(b)

FIGURE 5.20: The measured CMRR (a) and the Insertion Loss (b) of the baluns in Fig. 5.13.

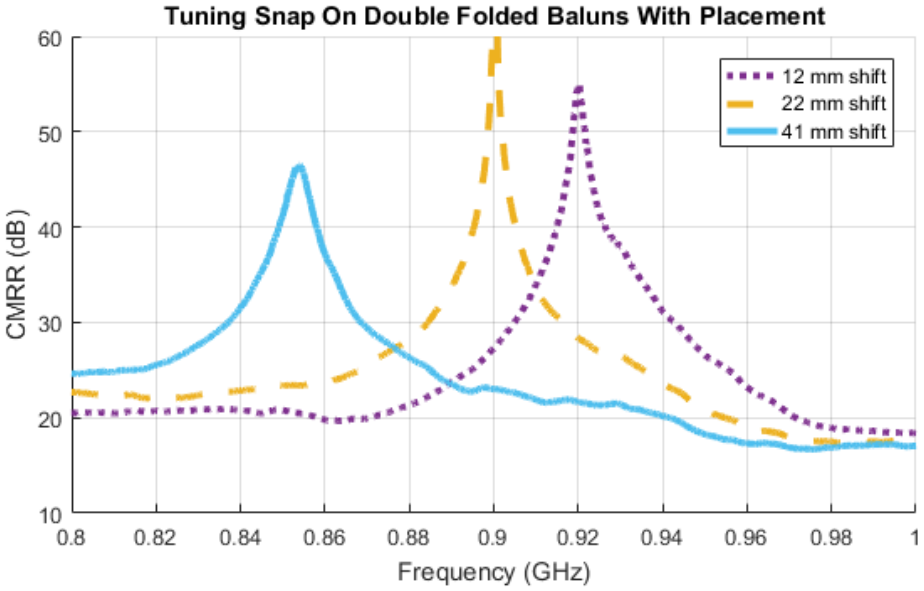

FIGURE 5.21: The measured CMRR data showing the tuning capability of changing the placement of the balun on the length of coax using the mesh double folded snap-on balun.

5.3.2 Dipole Radiation Patterns

In order to again test the actual functioning of these baluns, a number of the baluns were connected to dipole with the appropriate resonant frequency and the realized gain was measured in the E and H cut planes, giving the measured results in Fig. 5.22-5.26.

As can be seen in all of these results, the presence of the balun promoted more circular pattern in the H-plane cuts and deeper nulls in the E-plane cuts. The

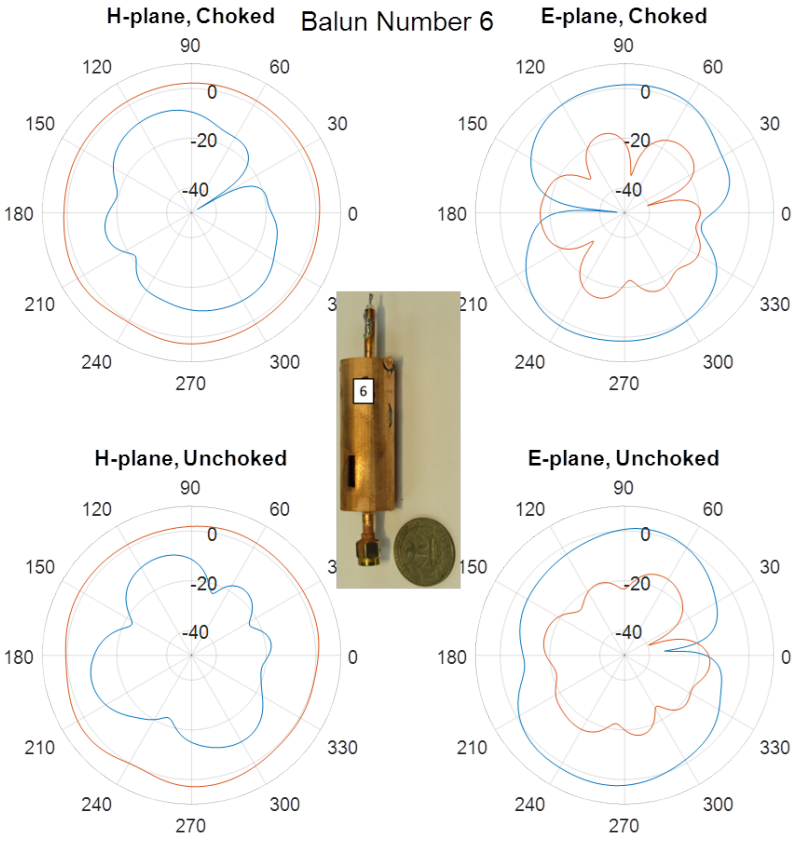

FIGURE 5.22: The measured radiation pattern of a dipole connected to a printed single folded balun at its operating frequency (top) and the measured radiation pattern of a dipole with no balun at the same frequency (bottom).

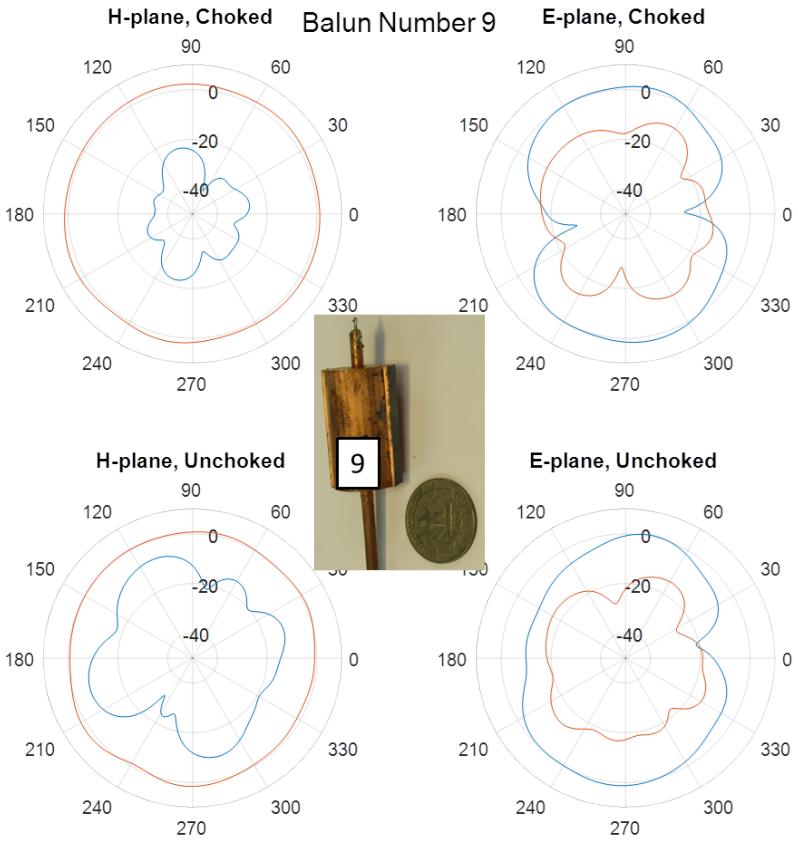

FIGURE 5.23: The measured radiation pattern of a dipole connected to a printed double folded balun at its operating frequency (top) and the measured radiation pattern of a dipole with no balun at the same frequency (bottom).

effects of not removing the supporting structures necessary for printing and plating can be seen in Fig. 5.26. The maximum realized gain has been significantly reduced, which suggests that there currents induced on the support structures that then cancelled the radiating fields from the dipole. This can be easily remedied by simply removing the supporting structures, as evidenced by the expected radiation characteristics seen in Fig. 5.23.

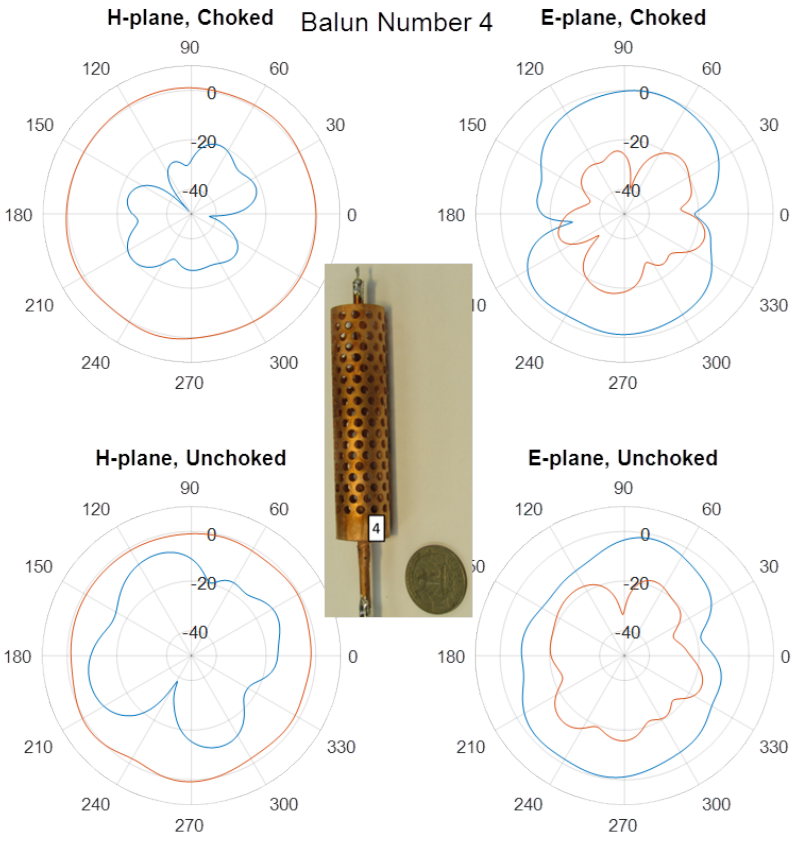

FIGURE 5.24: The measured radiation pattern of a dipole connected to a printed mesh unfolded balun at its operating frequency (top) and the measured radiation pattern of a dipole with no balun at the same frequency (bottom).

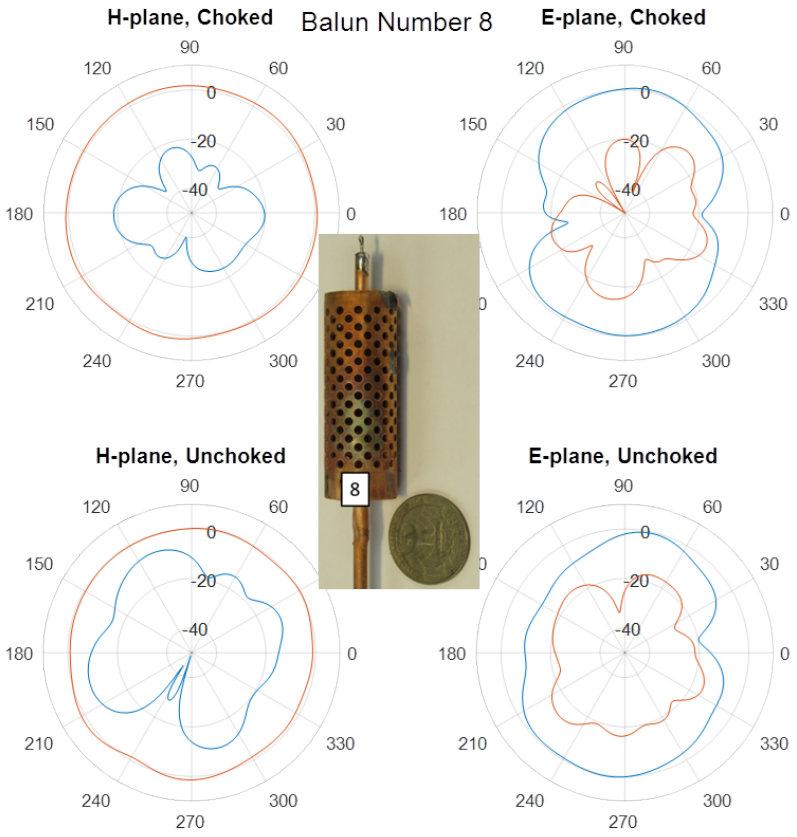

FIGURE 5.25: The measured radiation pattern of a dipole connected to a printed mesh single folded balun at its operating frequency (top) and the measured radiation pattern of a dipole with no balun at the same frequency (bottom).

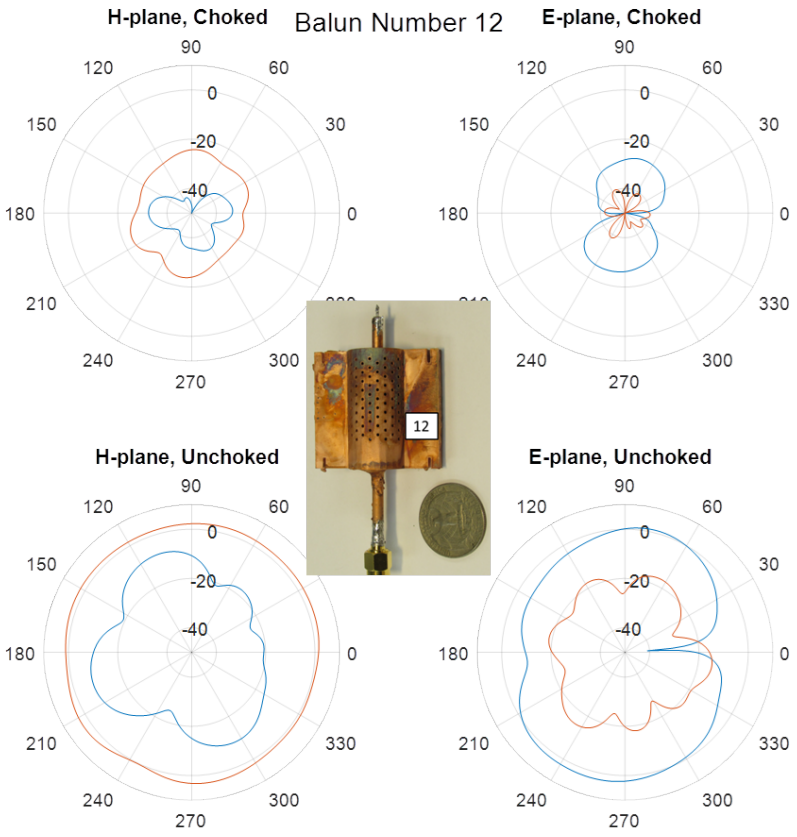

FIGURE 5.26: The measured radiation pattern of a dipole connected to a printed mesh double folded balun at its operating frequency (top) and the measured radiation pattern of a dipole with no balun at the same frequency (bottom).

5.4 Conclusions

In conclusion, the use of additive manufacturing for the creation of otherwise prohibitively difficult baluns was confirmed. Single and double folded baluns, both with solid and mesh walls, were designed and tested. All of the baluns tested shows greater than 38 dB of rejection at their operating frequency, confirming their functionality. The tuning capability of moving a balun to increase or decrease the space between the opening of the balun and the connection point of the balanced and unbalanced lines, with a tuning range of 70 MHz being achieved. The functionality of the baluns was also confirmed by measuring the realized gain of a dipole connected to each balun, with all of the baluns adequately choking the cable currents to achieve the desired dipole radiation pattern.

Chapter 6

Dielectrically Loaded Baluns

6.1 Background

A common method of reducing the size of microwave components in using a dielectric fill. This is widely used in Substrate Integrated Waveguides (SIW) to significantly reduce the overall size of the component [24–26]. This is possible because of the relation between the phase velocity and relative permittivity. It is well known that

$$\nu_p = \frac{1}{\sqrt{\mu\epsilon}}, \tag{6.1}$$

where ν_p is the phase velocity of a wave, μ is the permeability of a medium, and ϵ is the permittivity of a medium, and that

$$\lambda = \frac{\nu_p}{f}, \tag{6.2}$$

where λ is the wavelength of a wave and f is the frequency [14]. If the medium is free space, then Equation 6.1 becomes

$$\nu_p = \frac{1}{\sqrt{\mu_0 \epsilon_0}} = c, \tag{6.3}$$

where μ_0 is the permeability of free space, ϵ_0 is the permittivity of free space, and c is the speed of light. This is the source of the common relation

$$\lambda = \frac{c}{f}. \tag{6.4}$$

If the medium is anything other than free space, however, Equation 6.1 instead becomes

$$\nu_p = \frac{1}{\sqrt{\mu_0 \mu_r \epsilon_0 \epsilon_r}}, \tag{6.5}$$

where μ_r and ϵ_r are the relative permeability and permittivity of the medium respectively. Using this value for ν_p in Equation 6.2 then gives

$$\lambda = \frac{1}{\sqrt{\mu_0 \mu_r \epsilon_0 \epsilon_r} f} = \frac{1}{\sqrt{\mu_r \epsilon_r}} \frac{c}{f}. \tag{6.6}$$

Thus, by using a material with a higher relative permittivity or permeability, it is possible to significantly reduce the physical size of the component. For example, if a certain fraction of a wavelength would be 10 cm in one medium, it would be reduced to 2.5 cm in a medium with relative permittivity that is sixteen times greater. Equation 6.6 can also be rearranged to give

$$f = \frac{1}{\sqrt{\mu_r \epsilon_r}} \frac{c}{\lambda}, \tag{6.7}$$

which shows that if the physical wavelength, λ, is kept constant and the relative permittivity is increased, the frequency will decrease. This simple, yet powerful, property can then be applied to sleeve baluns to further reduce their size.

6.2 Printed Dielectric Cores

A simple method of creating a dielectrically loaded balun is to print a substrate core and add metal to it, creating the same effect detailed in Section 6.1. To test this, the substrate core seen in Fig. 6.1 was printed and attached to a length of semi-rigid coax. The ridges, which are the same ridge design as was used in the double folded balun design, create a snap fit to the semi-rigid coax, holding the core in place with nothing additional necessary. As a simple and inexpensive means of adding a conductor without the use of chemicals as Section 4, the printed core was then covered in a layer of basic adhesive-backed copper sheet, leaving one end uncovered. The balun, seen in Fig. 6.2, was then attached to the differential probe and tested.

A similar method can be used to create a folded balun with a printed core and adhesive copper sheet. In this case, the core is printed in four pieces and then the balun is assembled in layers. First the inner two portions of the core are attached to a length of semi-rigid coax. Next, the areas on the inner core indicated in orange in Fig. 6.3 are covered in adhesive-backed copper sheet. Then the outer two portions of the core are added to the inner core and, as was done previously, the areas indicated in Fig. 6.3 are covered in adhesive-backed copper sheet. The resulting balun can be seen in Fig. 6.4. This balun was then attached to the differential probe and tested.

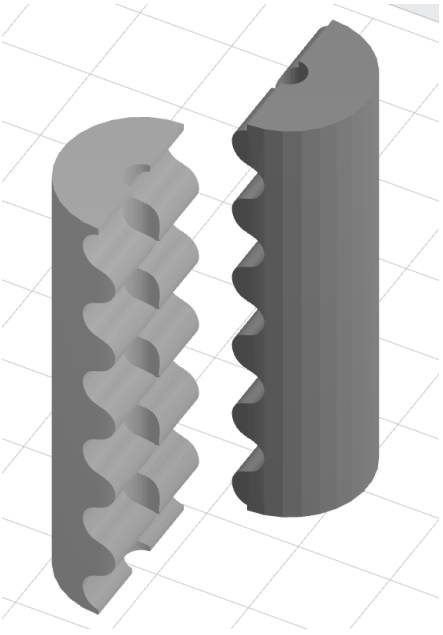

FIGURE 6.1: An example of the two halves of a printed core for an unfolded dielectrically loaded balun.

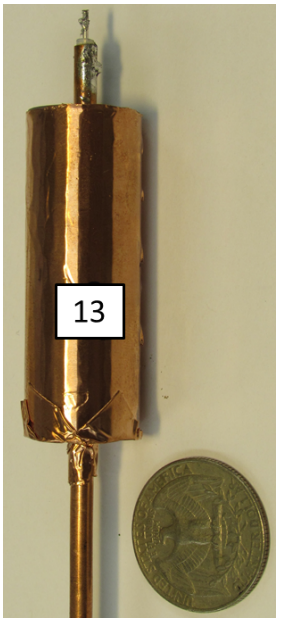

FIGURE 6.2: The final printed core dielectrically loaded unfolded balun with a standard American 25¢ coin for reference.

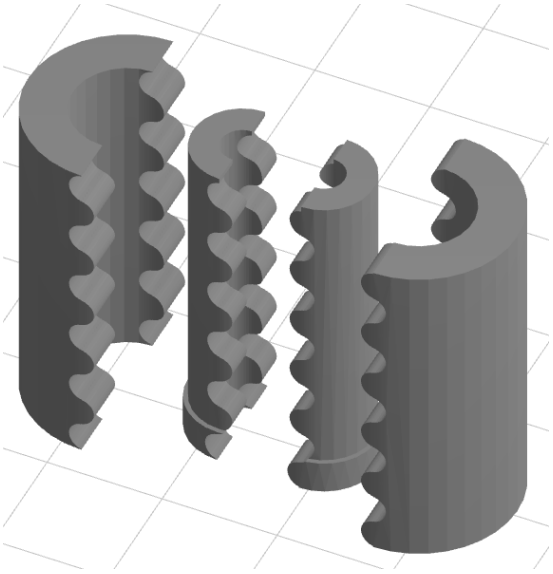

FIGURE 6.3: An example of a printed core for a single folded dielectrically loaded balun, expanded to show the parts.

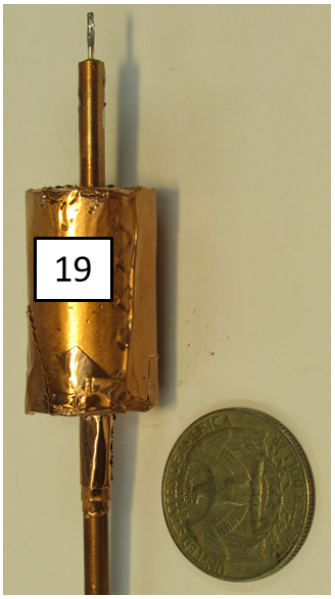

FIGURE 6.4: The final printed core dielectrically loaded single folded balun with a standard American 25¢ coin for reference.

6.2.1 Measurements

6.2.1.1 CMRR

The resulting measured CMRR for this printed core dielectrically loaded baluns can be seen in Fig. 6.5. The results show promise, given that there is a distinct peak at approximately the desired operational frequency of 915 MHz, but more work is needed. The adhesive-backed copper sheet was cut by hand and could be more accurately cut using an electronic die cutter, such as a Cricut [27]. This would improve the quality of the connections and refine several aspects such as the corners and the point where the adhesive-backed copper sheet connects to the coax.

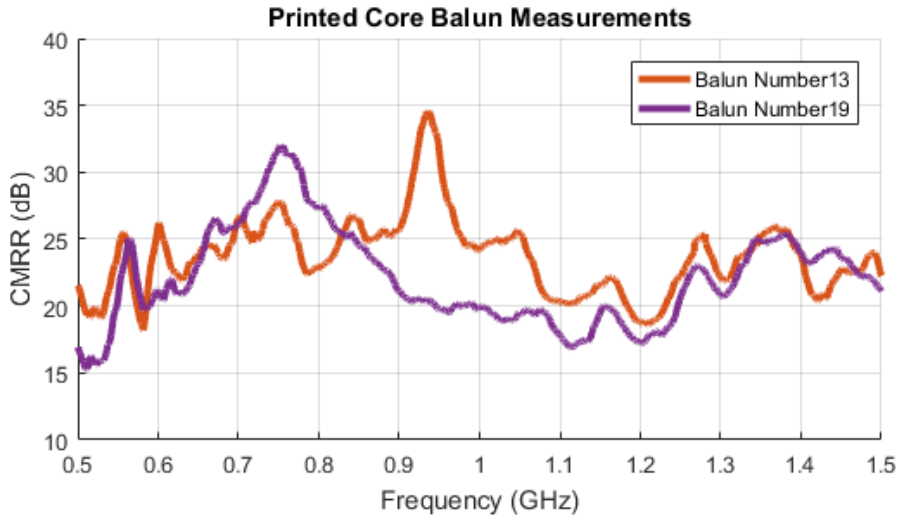

(a)

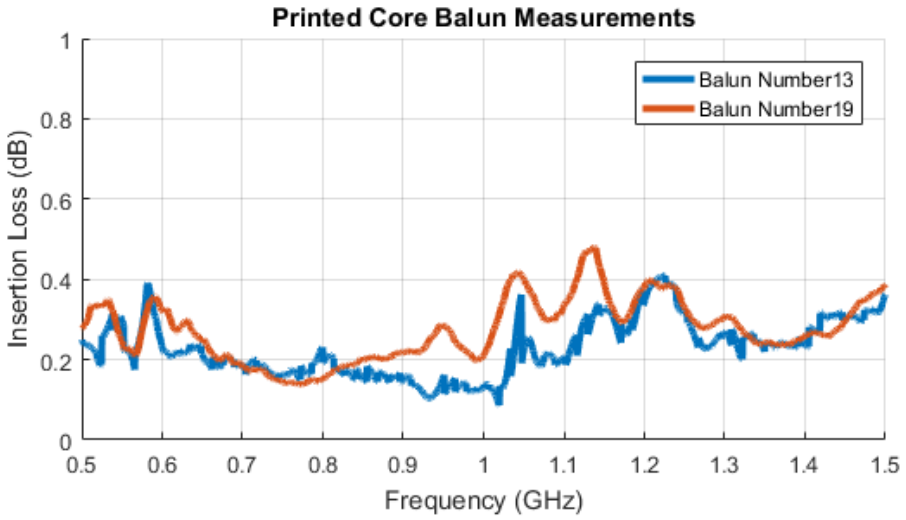

(b)

FIGURE 6.5: The measured CMRR (a) and Insertion Loss (b) for the two printed core dielectrically loaded baluns.

6.2.1.2 Dipole Radiation Patterns

The unfolded printed core balun was connected to a dipole with a matching operating frequency and the radiation characteristics of the dipole were measured as in previous chapters. Fig. 6.6 shows how the balun successfully reduced the cable currents and allowed for a smoother H-plane radiation pattern and deeper

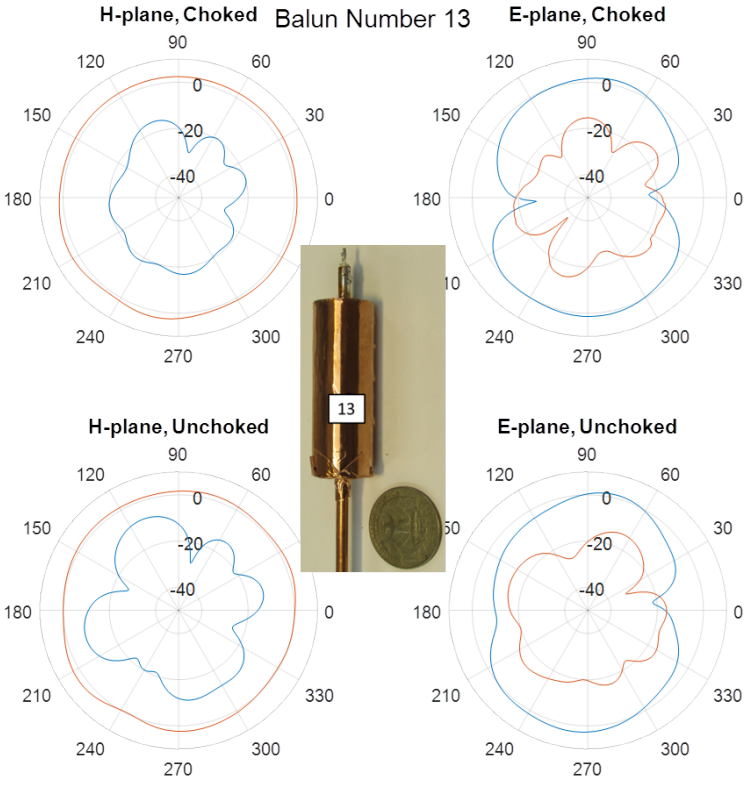

FIGURE 6.6: The measured radiation pattern of a dipole connected to a printed core unfolded balun at its operating frequency (top) and the measured radiation pattern of a dipole with no balun at the same frequency (bottom).

nulls in the E-plane radiation pattern.

6.3 Filling Existing Baluns

Another very simple method for changing the relative permittivity inside a balun is to fill the balun with an insulator. Castable silicone provides an easy means of accomplishing this. For a two-part silicone, which is a silicone that cures and hardens by a chemical process between two components that are mixed together, the silicone begins as a liquid initially and can be poured to fill any shaped desired. The silicone will then harden and hold that shape after following the

proper curing instructions, which will depend on the exact type of silicone and manufacturer instructions.

6.3.1 Copper Pipe Baluns

In order to verify the validity of this process, the method of filling an existing balun was first tested with standard sleeve baluns constructed out of copper pipe. These baluns were first cut to the same length and the CMRR was measured using the previously described method using the differential probe. Next, each balun was filled with a different type of silicone. Two types of silicone were selected for this test. Elastosil ®RT 601 and RT 604 are two two-part silicones, with relative permittivities of 2.8 and 2.6 respectively, were chosen because they have a nominal relative permittivity listed, which a large portion of commercial silicones do not [28, 29]. After curing the silicone according to the manufacturer instructions, the CMRR was measured again using the exact same method as before. The baluns after being filled with silicone can be seen in Fig. 6.7

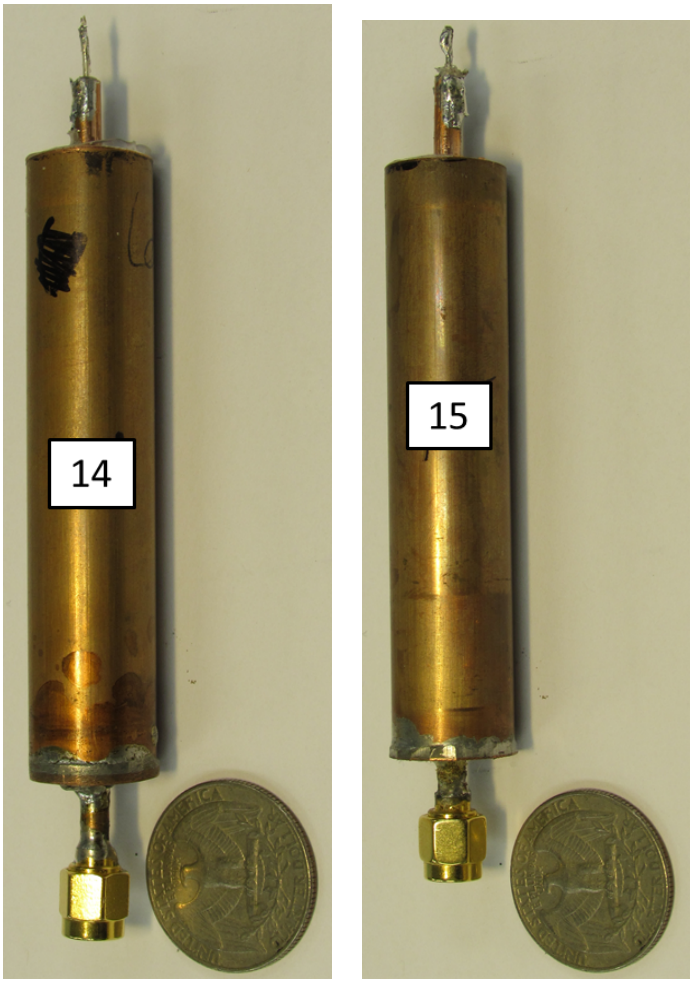

(a) (b)

FIGURE 6.7: The two baluns filled with Elastosil® RT 601 (a) and RT 604 (b), both with a standard American 25¢ coin for reference.

6.3.1.1 Measurements

6.3.1.2 CMRR

The CMRR measurements for both balun before and after being filled can be seen in Fig. 6.8. As these measurements clearly show, the operating frequency of the baluns has been drastically reduced. These results strongly agree with the expectations derived from Equation 6.7. The actual effective relative permittivity of each silicone can be found by taking the square of the ratios of the operating

frequencies before and after being filled for each balun respectively, with the RT 601 filled balun going from 949.1 MHz to 565.8 MHz and the RT 604 filled balun going from 838.2 MHz to 568.7 MHz. Doing so gives a relative permittivity of 2.86 and 2.15 for the RT 601 and RT 604, respectively. These values are well within expectations. A combination of minor frequency shifts from the slight differences in where the differential probe was connected and trapped air in the silicone can lead to a slightly over- or under-estimated value. As can drastically be seen in Figure 6.10, this silicone is prone to air bubbles, which will lower the relative permittivity to some value between the relative permittivities of air and the silicone according to effective medium approximations, such as the Maxwell Garnett equation, which states

$$(\frac{\epsilon_{eff} - \epsilon_m}{\epsilon_{eff} + 2\epsilon_m}) = \delta_i(\frac{\epsilon_i - \epsilon_m}{\epsilon_i + 2\epsilon_m}), \tag{6.8}$$

where ϵ_{eff} is the effective relative permittivity of the medium, ϵ_m is the relative permittivity of the silicone in this case, ϵ_i is the relative permittivity of air in this case, and δ_i is the percent volume that is occupied by air [30]. The inclusion of air in this way could be used to strategically control the relative permittivity of the medium, but this is beyond the scope of this thesis. The reduced peak CMRR value in Fig. 6.7(b) is from the decreased quality of connections from excess silicone that escaped the balun walls.

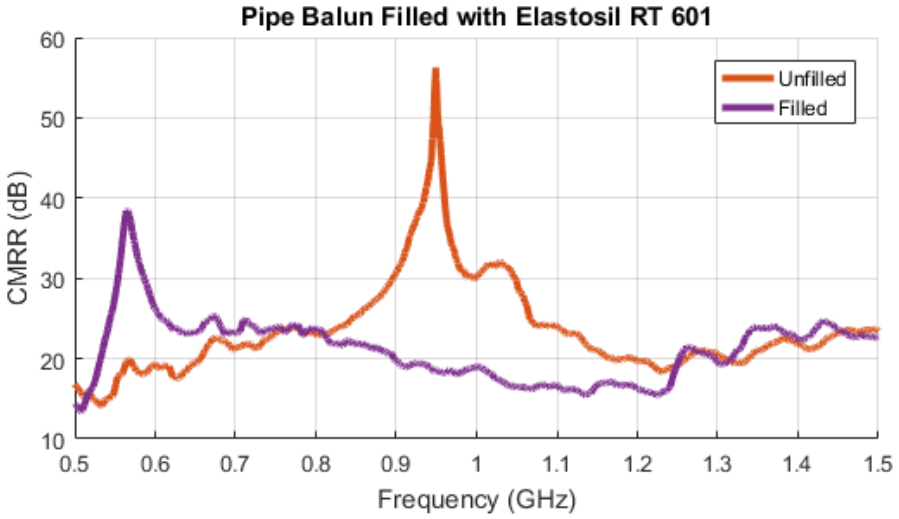

(a)

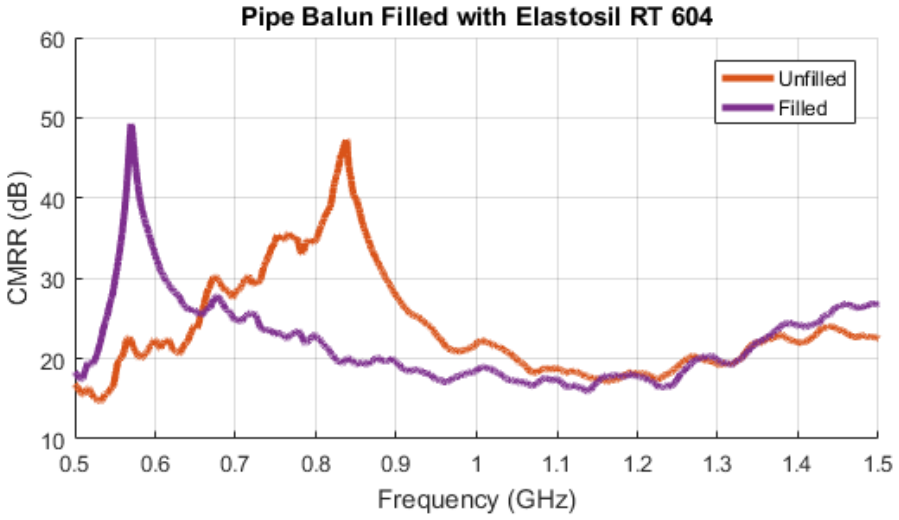

(b)

FIGURE 6.8: The CMRR measurements for two pipe baluns before being filled with Elastosil ®RT 601 (a) and RT 604 (b) and the Insertion Loss for both baluns (c).

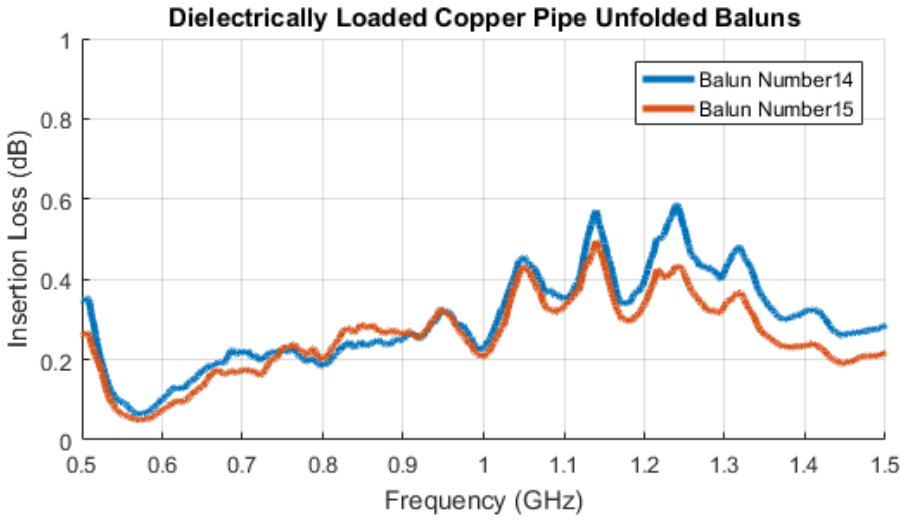

FIGURE 6.9: The Insertion Loss of the filled copper pipe baluns in Fig. 6.8.

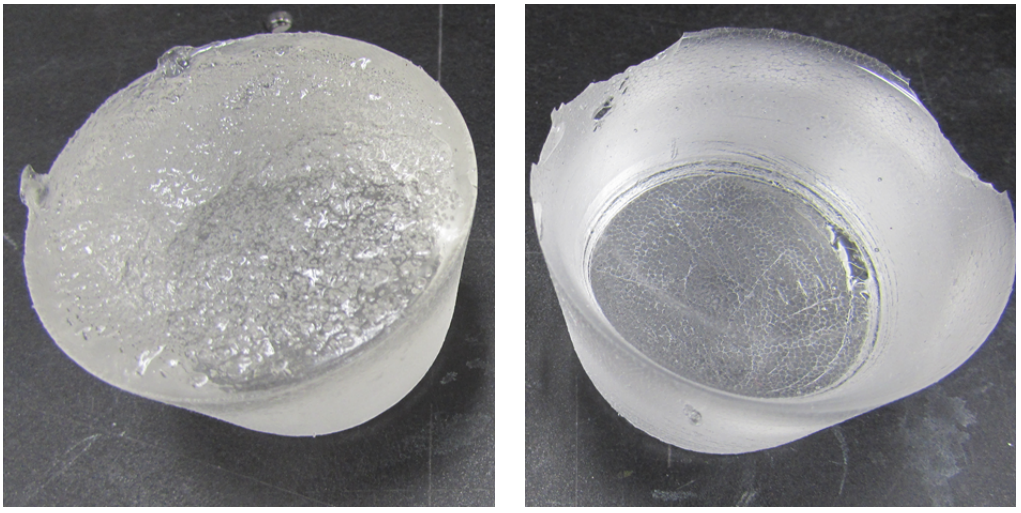

(a) (b)

FIGURE 6.10: Example samples of Elastosil ®RT 601 (a) and RT 604 (b). Note the larger amount of air bubbles and rougher finish in the RT 601, which would lead to a relative permittivity different from the nominal value.

6.3.1.3 Dipole Radiation Patterns

The balun filled with RT 604 was connected to an appropriately sized dipole and the realized gain was measured in the same method as the previous chapters. As seen in Fig. 6.11, the balun promotes a dipole radiation pattern similar to those in previous chapters.

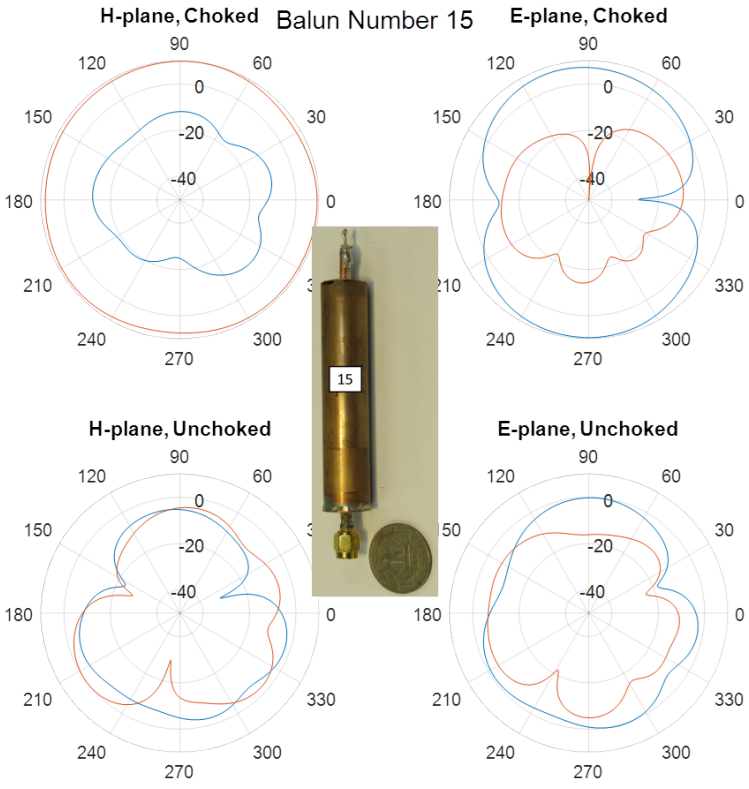

FIGURE 6.11: The measured radiation pattern of a dipole connected to a dielectrically loaded copper pipe unfolded balun at its operating frequency (top) and the measured radiation pattern of a dipole with no balun at the same frequency (bottom).

6.3.2 Filled Printed, Folded Baluns

The size reduction effects of a dielectric fill can be compounded with the size reduction from folding the balun. To push this miniaturization to its extreme, two double folded balun were filled with with Elastosil ®RT 604. RT 604 was chosen over RT 601 because of its higher quality finish. First, the double folded mesh balun design was reduced in length by $\frac{1}{\sqrt{\epsilon_r}}$, which is roughly 40% in this case, in order to maintain the same operating frequency as the unfilled design according to Equation 6.6. Two of these double folded mesh baluns, with the mesh aspect being chosen to ensure complete plating throughout, were printed and plated, keeping the halves separate. The sets of halves were then secured to two lengths of semi-rigid coax using quick-curing epoxy, with extra epoxy being applied to create a water tight seal at the connection point of the balun halves. Next, the two baluns were then sealed and filled in two different ways. For the first, the holes on the sides of the balun were sealed using electrical tape such that the only opening in the balun was where the coax exits the balun, opposite the point of connection. This balun was filled by pouring silicone down into this hole. For the second balun, all of the openings on the top, one side, and part of one side were sealed with electrical tape such that only two rows of holes were visible. This balun was then filled with silicone using a syringe inserted into the exposed holes. The final filled, double folded mesh baluns can be seen in Fig. 6.12. These baluns were then connected to the differential probe and tested in the same method as all of the previous baluns.

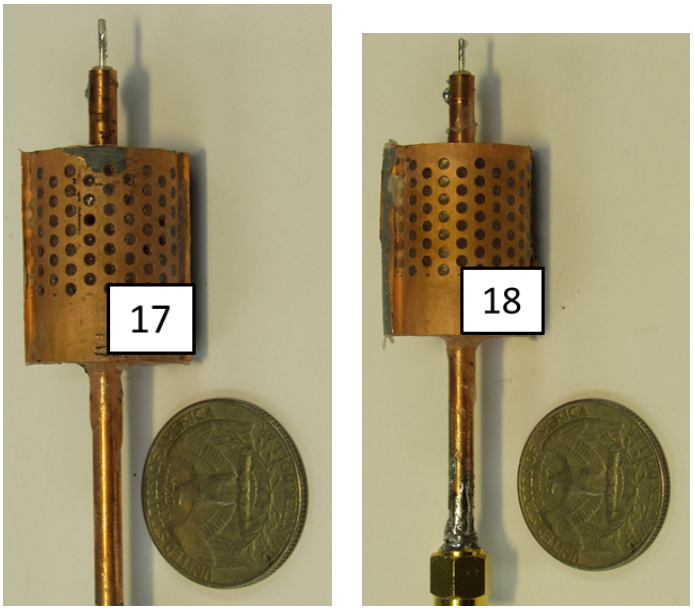

(a) (b)

FIGURE 6.12: The two dielectrically loaded, double folded mesh baluns, with (a) being the topped filled balun and (b) being the syringe filled balun, both with a standard American 25¢ coin for reference.

6.3.2.1 Measurements

6.3.2.2 CMRR

The measured CMRR for the dielectrically loaded, double folded mesh baluns detailed in Section 6.3.2 can be seen in Fig. 6.13. The reduced and shifted peak rejection of the balun filled from the top as compared to the balun filled from the side is most likely due to trapped air in the corners of the balun that can cause mixed material effects and spurious modes to form. Importantly, though, these results show that a dielectrically loaded, double folded balun is indeed a viable option for use as a balun at low frequencies while maintaining a small form factor. An illustration of this small form factor can be seen in Fig. 6.14 where the balun is compared to a common ferrite bead found on a laptop power cable.

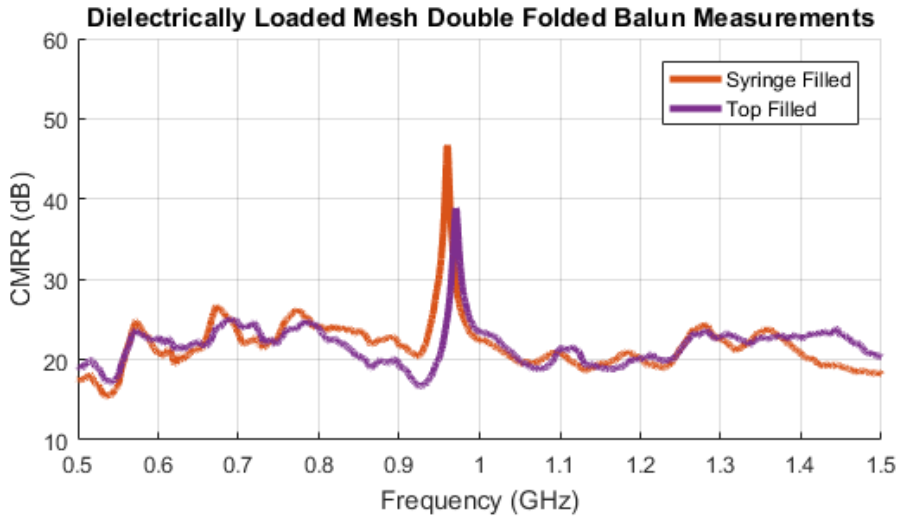

(a)

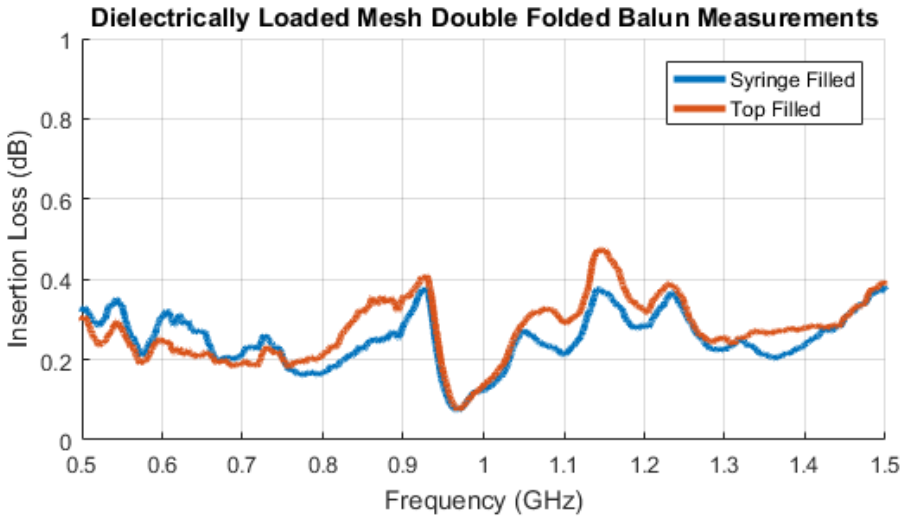

(b)

FIGURE 6.13: The measured CMRR (a) and Insertion Loss (b) of the two dielectrically loaded, double folded mesh baluns.

The filled double folded balun is 26.3 mm long, whereas an unfolded balun at the same frequency would be 78.1 mm long, illustrating the extreme size reduction.

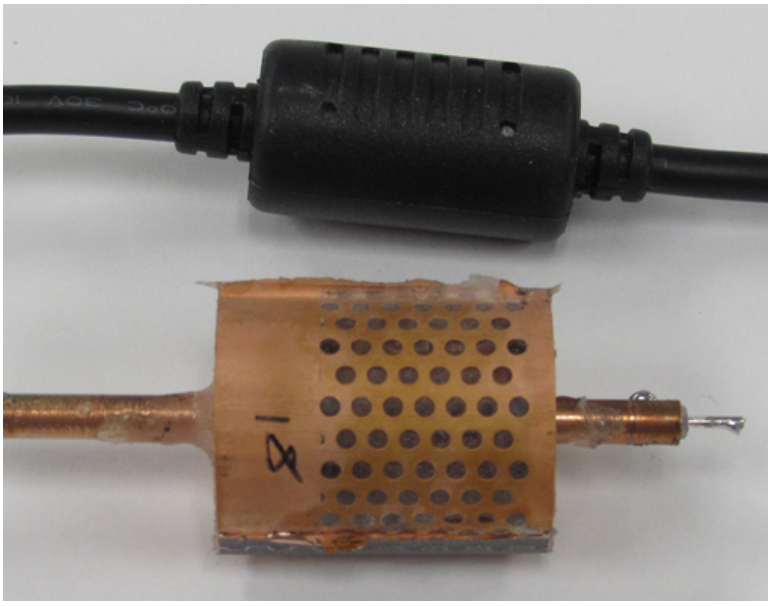

FIGURE 6.14: An illustration of the size reduction possible with a dielectrically loaded, double folded mesh balun, shown next to a ferrite bead on a laptop power cable.

6.3.2.3 Dipole Radiation Patterns

One of the dielectrically loaded printed double folded mesh baluns was connected to a dipole and the realized gain was measured in the same fashion as in previous chapters, giving the plots seen in Fig. 6.15. As can be seen in this figure, the balun functioned similarly to the prevous baluns and choked the cable currents, resulting in a more desired dipole radiation patter.

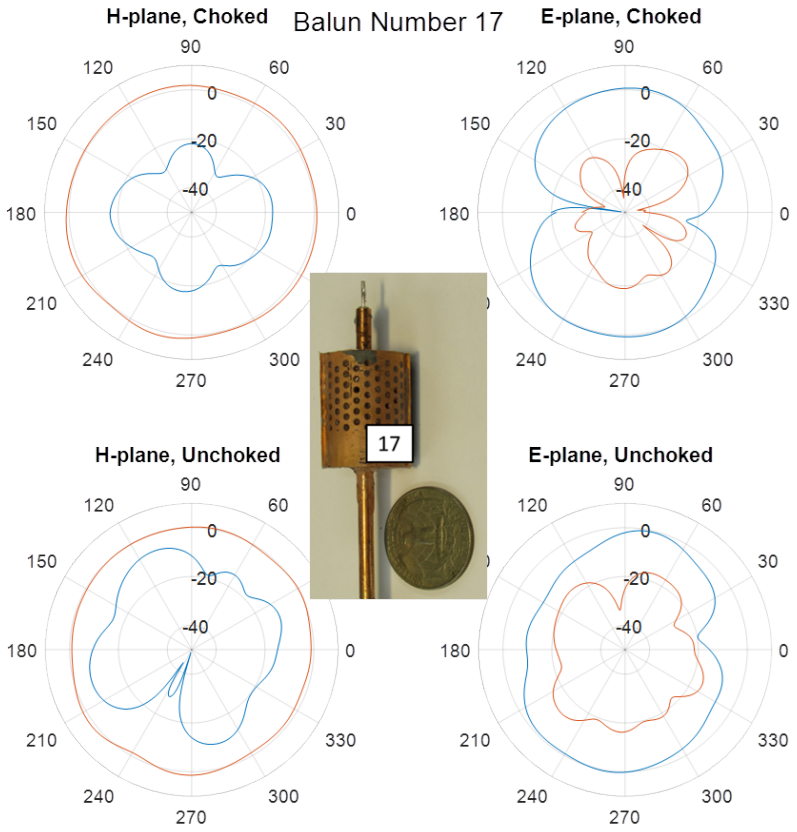

FIGURE 6.15: The measured radiation pattern of a dipole connected to a dielectrically loaded printed mesh double folded balun at its operating frequency (top) and the measured radiation pattern of a dipole with no balun at the same frequency (bottom).

6.4 Conclusions

Several baluns with reduced size by dielectric loading were presented. The first and second baluns used a combination of a 3D printed dielectric core and adhesive-backed copper sheet to create simple, inexpensive baluns. The first of this type, seen in Fig. 6.2, had a printed core that could snap to a length of semi-rigid coax. This core was then covered in adhesive-backed copper sheet to form a dielectrically loaded unfolded balun. The next balun used a similar method, but

required more careful assembly. It consisted of a set of core pieces that were connected to a length of semi-rigid coax and carefully covered with adhesive-backed copper sheet in a strategic manner to form a dielectrically loaded single folded balun. These two baluns show promise, but more future work would be needed to refine them and increase their level of rejection to level on par with the other baluns.

Next, the third type, which were constructed out of copper pipe and filled with silicone, show that an existing balun's operating frequency can be adjusted and controlled through the use of a dielectric fill. As can be seen in Fig. 6.8, these baluns follow the expected behavior almost exactly with only slight variations. The fourth baluns then combined the size reduction from folding with the size reduction from a dielectric infill. These dielectrically loaded, double folded mesh baluns achieved greater than 38 dB of rejection at their operating frequency in a form factor roughly the same size as a common ferrite bead. These filled baluns also have the added benefit of increased structural integrity compared to their unfilled counterparts as the slightly flexible silicone acts as a shock absorber.

Chapter 7

Conclusions & Future Work

7.1 Conclusion

In many RF and microwave applications, a balanced structure must inevitably be connected to an unbalanced structure due to the ubiquitous use of coaxial cable. Therefore, a balun is imperative at this point of connection in order to prevent unwanted impedance mismatches, reflections, and radiative cable currents. A common type of balun for use with coaxial cable is a sleeve balun. These baluns are straightforward structures, but they are bulky, heavy, and time-intensive to make. The work presented here improved on these baluns in several ways using additive manufacturing techniques, including size, weight, and manufacturing capabilities. The process of using additive manufacturing to create a sleeve balun was first validated by printing and copper plating an unfolded sleeve balun to act as a direct comparison to traditionally manufactured sleeve baluns. These printed baluns have the benefits of being significantly lighter weight and can be produced in large batches with no significant increase in time requirements and

have comparable performance compared to baluns made from copper pipe. Folding sleeve baluns a single time in order to reduce their size has been established in [5, 6], but these baluns are even more difficult to construct than their unfolded counterparts. Therefore, the additive manufacturing techniques verified using unfolded baluns were then applied to single folded baluns. Folding these baluns resulted in a 40% reduction is size while maintaining the same level of performance. These techniques were then extended to double folded baluns, which had not been investigated at all prior to this due to the prohibitive difficulty of their construction. Thus, a novel, double folded balun design was created, with several aspects being designed to promote improved print and plating quality. The second fold added another 40% reduction in size comparable to the single folded baluns, resulting in an overall 64% reduction in the size of the balun compared to an unfolded balun with equivalent levels of rejection.

Another method of size reduction used in RF and microwave technologies is using a dielectric fill to decrease the wavelength in a region. This technique was first applied to copper pipe baluns, where two traditionally manufactured copper pipe baluns were filled with castable silicone. The results from before and after being filled show almost exactly the expected decrease in frequency for this physical size. This technique was then applied to double folded baluns. This results in a 78.5% size reduction compared to similar unfilled, unfolded baluns and are of a similar size and form factor to that of commonly used ferrite beads, while still achieving comparable performance to that of any other balun.

The final type of balun tested used a printed core to achieve the same reduction in size with increased relative permittivity. These baluns consisted of a printed core that was then strategically and carefully covered with adhesive-backed copper sheet. While the performance of these baluns was not at the same level as the

previous baluns, these baluns still show promise as an inexpensive and accessible alternative.

All of the baluns presented in this work are listed in Tables 7.1-7.3 with their production method, wall type, fill type, height, diameter, number of folds, attachment method, placement spacing, max rejection, and operating frequency.

Balun Number	Method	Wall Type	Fill	Height (mm)	Diameter (mm)
1	pipe	solid	none	83.56	16
2	print	solid	none	74.87	19.2
3	print	solid	none	75	19.1
4	print	mesh	none	80.52	19.1
5	print	solid	none	53.9	19.4
6	print	solid	none	52.3	19.1
7	print	solid	none	46.7	19.1
8	print	mesh	none	53.45	19.1
9	print	solid	none	33.77	19.4
10	print	solid	none	38	19.7
11	print	solid	none	38.4	28.1
12	print	mesh	none	38	19.2
13	print	tape	printed core	50.4	18.1
14	pipe	solid	601	78	15.9
15	pipe	solid	604	77.4	15.9
16	print	mesh	none	38	19.5
17	print	mesh	601top	26.3	19.6
18	print	mesh	601syringe	26.6	19.6
19	print	tape	printed core	30.8	18.1

TABLE 7.1: Table of All Balun Parameters

Balun Number	Number of Folds	Attachment Method	Placement Spacing (mm)
1	0	solder	10
2	0	glue/plate	13.14
3	0	glue/plate	14
4	0	glue/plate	10
5	1	plate/silver	23.4
6	1	glue/plate	18.2
7	1	glue/plate	17.7
8	1	glue/plate	10
9	2	glue/plate	10
10	2	snap	variable
11	2	segment	10.8
12	2	glue/plate	10.8
13	0	snap core	10
14	0	solder	9.4
15	0	solder	12.2
16	2	snap	variable
17	2	plate/glue	10.5
18	2	plate/glue	10.4
19	1	snap core	17.2

TABLE 7.2: Table of All Balun Parameters (Continued)

Balun Number	Max Rejection (dB)	Operating Frequency (GHz)	Insertion Loss (dB)
1	67.26	0.837	0.0472
2	40.69	0.857	0.0866
3	39.5	0.912	0.2261
4	49.82	0.974	0.0604
5	54.71	0.779	0.4495
6	39.47	0.913	0.1956
7	50.39	0.918	0.1845
8	50.25	0.958	0.0611
9	49.7	0.948	0.0917
10	48.55	0.864	0.0689
11	41.97	0.927	0.1848
12	41.16	0.900	3.05E-04
13	34.5	0.932	0.1066
14	38.45	0.561	0.0691
15	49.26	0.572	0.05
16	42.93	0.915	0.0705
17	46.73	0.959	0.0848
18	38.86	0.970	0.0789
19	31.98	0.751	0.1437

TABLE 7.3: Table of All Balun Parameters (Continued)

7.2 Future Work

Many of these techniques can still be refined and expanded upon, leading to many opportunities for future work. For example, a number of folds greater than two could be investigated. The primary consideration as the number of folds increases is maintaining a balance of size and wall thickness to maintain structural integrity. As the number of folds increases either the wall thickness must decrease, which increases the likelihood of print defects and structural failure, or the overall diameter must increase, which begins to run counter to the goal of decreasing the overall size of the balun. Another avenue of future work would be to utilize the plethora of holes in the mesh balun designs to insert other conductive elements into the interior of the balun. These elements could be used to tune the operating frequency of the balun, create multiple operating frequencies, or even create a broader bandwidth sleeve balun. Similarly, the silicone in the substrate integrated baluns could be used to suspend other elements. While these elements could not be tuned, they would allow for the creation of much more complex designs. A dielectric core could also be printed and inserted into the folded baluns prior to being attached to the semi-rigid coax. Parameters of this core could be more finely controlled than the silicone, but all print aspects must be exactly precise with not defects for everything to be assembled properly. Finally, the printed core substrate integrated baluns could be significantly improved and refined with the use of automated die-cutters, such as a Cricut, and other quality control processes.

Bibliography

[1] Seppo Saario, DV Thiel, JW Lu, and SG O'Keefe. An assessment of cable radiation effects on mobile communications antenna measurements. In *Antennas and Propagation Society International Symposium, 1997. IEEE., 1997 Digest*, volume 1, pages 550–553. IEEE, 1997.

[2] P. J. Massey and K. R. Boyle. Controlling the effects of feed cable in small antenna measurements. In *Twelfth International Conference on Antennas and Propagation, 2003 (ICAP 2003). (Conf. Publ. No. 491)*, volume 2, pages 561–564 vol.2, March 2003.

[3] C.A. Balanis. *Advanced Engineering Electromagnetics*. CourseSmart Series. Wiley, 2012. ISBN 9780470589489.

[4] C.A. Balanis. *Antenna theory: analysis and design*. John Wiley & Sons, 3 edition, 2005.

[5] Clemens Icheln, Joonas Krogerus, and Pertti Vainikainen. Use of balun chokes in small-antenna radiation measurements. *IEEE Transactions on Instrumentation and Measurement*, 53(2):498–506, 2004.

[6] Matthew Slater. *Design and analysis of direction-of-arrival estimation systems using electrically small antenna arrays*. PhD thesis, University of Illinois at Urbana-Champaign, 2012.

[7] Icheln C., Popov M., Vainikainen P., and He S. Optimal reduction of the influence of rf feed cables in small antenna measurements. *Microwave and Optical Technology Letters*, 25(3):194–196, 1999. doi: 10.1002/(SICI)1098-2760(20000505)25:3⟨194::AID-MOP11⟩3.0.CO;2-\#.

[8] J. DeMarinis. The antenna cable as a source of error in emi measurements. In *IEEE 1988 International Symposium on Electromagnetic Compatibility*, pages 9–14, Aug 1988.

[9] S. A. Saario, J. W. Lu, and D. V. Thiel. Full-wave analysis of choking characteristics of sleeve balun on coaxial cables. *Electronics Letters*, 38(7): 304–305, Mar 2002.

[10] *Round Cable Snap-Its*. Fair-Rite Products Corp., 3 2018.

[11] R Skelton. Measuring HF balun performance. In *QEX*, number 263, pages 39–41, 2010.

[12] ANSYS. High frequency structure simulator, 2016.

[13] David Keun Cheng et al. *Field and Wave Electromagnetics*. Pearson Education India, 1989.

[14] David M Pozar. *Microwave engineering*. John Wiley & Sons, 2012.

[15] Jessica Ruyle. *Small, dual band, placement insensitive antennas*. PhD thesis, University of Illinois at Urbana-Champaign, 2012.

[16] S. Johann, F. William, P. Aurélien, T. Olivier, D. Nicolas, S. Bila, V. Serge, P. Jean-Baptiste, and R. P. Gramond. Plastic and metal additive manufacturing technologies for hyperfrequency passive components up to Ka band. In *2016 46th European Microwave Conference (EuMC)*, pages 373–376, Oct 2016. doi: 10.1109/EuMC.2016.7824356.

[17] P. Booth and E. V. Lluch. Enhancing the performance of waveguide filters using additive manufacturing. *Proceedings of the IEEE*, 105(4):613–619, April 2017. ISSN 0018-9219. doi: 10.1109/JPROC.2016.2616494.

[18] M. D. Benge, R. C. Huck, and H. H. Sigmarsson. X-band performance of three-dimensional, selectively laser sintered waveguides. In *2014 IEEE Antennas and Propagation Society International Symposium (APSURSI)*, pages 13–14, July 2014. doi: 10.1109/APS.2014.6904338.

[19] A. I. Dimitriadis, T. Debogović, M. Favre, M. Billod, L. Barloggio, J. P. Ansermet, and E. de Rijk. Polymer-based additive manufacturing of high-performance waveguide and antenna components. *Proceedings of the IEEE*, 105(4):668–676, April 2017. ISSN 0018-9219. doi: 10.1109/JPROC.2016.2629511.

[20] M. D'Auria, W. J. Otter, J. Hazell, B. T. W. Gillatt, C. Long-Collins, N. M. Ridler, and S. Lucyszyn. 3-D printed metal-pipe rectangular waveguides. *IEEE Transactions on Components, Packaging and Manufacturing Technology*, 5(9):1339–1349, Sept 2015. ISSN 2156-3950. doi: 10.1109/TCPMT.2015.2462130.

[21] *Tech Specs for the Form 2*. Formlabs, 2017.

[22] *Electroless Copper 4000 Process*. OM Group Electronic Chemicals LLC, 8 2017.

[23] Formlabs. Preform, 2018.

[24] D. Deslandes and K. Wu. Integrated microstrip and rectangular waveguide in planar form. *IEEE Microwave and Wireless Components Letters*, 11(2): 68–70, Feb 2001. ISSN 1531-1309. doi: 10.1109/7260.914305.

[25] D. Deslandes and Ke Wu. Accurate modeling, wave mechanisms, and design considerations of a substrate integrated waveguide. *IEEE Transactions on Microwave Theory and Techniques*, 54(6):2516–2526, June 2006. ISSN 0018-9480. doi: 10.1109/TMTT.2006.875807.

[26] Feng Xu and Ke Wu. Guided-wave and leakage characteristics of substrate integrated waveguide. *IEEE Transactions on Microwave Theory and Techniques*, 53(1):66–73, Jan 2005. ISSN 0018-9480. doi: 10.1109/TMTT.2004.839303.

[27] Cricut maker. URL https://home.cricut.com/cricut-maker.

[28] *Elastosil RT 601 A/B*. Wacker Chemical Corporation., 11 2017.

[29] *Elastosil RT 604 A/B*. Wacker Chemical Corporation., 11 2017.

[30] Tuck C Choy. *Effective medium theory: principles and applications*, volume 165. Oxford University Press, 2015.